

Event generation at MEPS@NLO accuracy in neutral and charged current DIS at the EIC

Peter Meinzinger^{*1}, Daniel Reichelt^{†2}, and Federico Silveti^{‡3}

¹*Physik-Institut, Universität Zürich, Winterthurerstrasse 190, CH-8057 Zürich, Switzerland*

²*CERN, Theoretical Physics Department, CH-1211 Geneva 23, Switzerland*

³*Institute for Particle Physics Phenomenology, Department of Physics, Durham University, Durham DH1 3LE, United Kingdom*

Abstract: We present the first hadron-level predictions at MEPS@NLO precision for both neutral and charged current DIS at the EIC and the first application of the MEPS@NLO technique to charged current DIS in general. We critically examine state-of-the-art inclusive predictions using multi-leg merging techniques, contrasting perturbative and non-perturbative uncertainties. We study typical kinematic DIS observables as well as jet measurements and 1-jettiness with realistic cuts implied by expected and past detector resolution. On the perturbative side, we see large corrections towards small virtualities and Bjorken- x , which can be captured by higher-multiplicity matrix elements and the merging procedure. Non-perturbative effects, while negligible in most jet observables, can reach similar size as the perturbative uncertainties around the peak of the 1-jettiness distributions especially at low values of Q^2 .

*Email: peter.meinzinger@uzh.ch

†Email: d.reichelt@cern.ch

‡Email: federico.silvetti@durham.ac.uk

Contents

1	Introduction	2
2	Overview of DIS kinematics and analyzed observables	3
3	Event Generation for DIS in SHERPA	5
3.1	MEPS@LO, MC@NLO and MEPS@NLO	5
3.2	Systematic uncertainties of event generation in DIS	6
4	Event Generation for HERA and MEPS@NLO in charged current DIS	7
5	Event generation for the EIC and its systematic uncertainties	9
5.1	Neutral Current	10
5.2	Charged Current	15
6	Conclusion	20
A	Further Observables	21
A.1	Neutral current 1-jettiness	21
A.2	Charged current 1-jettiness	23
A.3	Charged current groomed 1-jettiness	24

1 Introduction

Lepton-hadron collision experiments, as conducted for example at HERA, are crucial for probing hadron structure [1–3]. These interactions occur via the exchange of at least one electroweak boson. When the virtuality of this mediator is sufficiently large, i.e., $Q^2 \gg m_p^2 \sim 1 \text{ GeV}^2$, the interaction enters the Deeply Inelastic Scattering (DIS) regime. In this limit, the factorization of the cross-section into matrix elements and parton distribution functions (PDFs) has been proven explicitly [4, 5], hence allowing the application of perturbative techniques. Specifically, in the case of neutral-current (NC) DIS mediated by photons and Z-bosons, in contrast to charged-current (CC) DIS mediated by W-bosons, measurements can be performed fully inclusively with respect to the hadronic final state, providing a high-precision probe of the proton’s partonic structure.

In recent years, lepton-hadron scattering has garnered more attention again due to the upcoming planned for the Electron-Ion Collider (EIC) at Brookhaven National Laboratory. The EIC aims for unprecedented precision in determining the spatial and transverse-momentum distributions of partons in the proton [6, 7]. Maximizing the available statistics for experimental analyses requires lowering the virtuality cut-off, as the cross-section scales as $1/Q^4$. However, at lower Q^2 , additional scales – such as jet transverse momenta – can become dominant, leading to increased theoretical uncertainties. This challenge is addressed by the computation of higher-order corrections in fixed-order (FO) perturbation theory, particularly via real radiation corrections in QCD. While current FO calculations extend up to N³LO [8–10], further improvements are computationally prohibitive in the foreseeable future. Additionally, the lower center-of-mass energy than, *e.g.*, at HERA shifts the attention toward smaller values of Q^2 as well as non-perturbative corrections which should approximately be of the order Λ_{QCD}/Q or $\Lambda_{\text{QCD}}^2/Q^2$.

An alternative approach is multi-jet merging, which combines tree-level matrix elements of varying final-state multiplicities and parton shower evolution. This method was initially developed at leading order (LO) [11, 12] and later extended to next-to-leading order (NLO) [13, 14]. Multi-jet merging for DIS

was recently also studied at LO within the PYTHIA event generator [15], too. Although not a complete higher-order correction, this approach effectively captures the dominant effects at small virtualities, in particular in the range $Q^2 \simeq \mathcal{O}(1\text{-}10 \text{ GeV}^2)$.

Most previous studies of inclusive DIS phenomenology for the EIC have relied on LO calculations, primarily using PYTHIA [16–22]. Notably, Ref. [16] explored the full- Q^2 phase space, including the low- Q^2 photoproduction regime at LO. DIS has also been recently studied at matched NLO accuracy in the POWHEG formalism in Refs. [23–25]. Several other tools [26, 27] are available to compute DIS observables at NNLO accuracy for the EIC. Furthermore, jet predictions in the photoproduction regime were computed at NLO in Ref. [28], see also Ref. [29].

In this work, we present a study of precision DIS phenomenology at the EIC using the SHERPA event generator. Specifically, we employ its automated matching and merging capabilities to produce the most precise, fully exclusive hadron-level predictions to date. We analyze both traditional DIS observables and hadronic event shapes, including 1-jettiness, jet multiplicities, and leading-jet transverse momentum. To assess theoretical uncertainties, we perform independent evaluations of perturbative and non-perturbative effects, identifying limitations in theoretical predictions relevant to EIC analyses.

We structure our paper as follows: In Sec. 2, we introduce our notation for DIS kinematics and define the observables to be studied. Sec. 3 details our simulation framework within SHERPA, and Sec. 4 presents a validation of the CC DIS simulation against ZEUS data. We then analyze NC and CC DIS events at the EIC in Sec. 5, before concluding in Sec. 6.

2 Overview of DIS kinematics and analyzed observables

We consider DIS events between an electron and a proton with momentum p and P respectively,

$$e^-(p) + p(P) \rightarrow l(p') + X(p_X) \quad (1)$$

This results in collection of hadrons with momentum p_X plus a recoiling fermion momentum p' which can be either another electron, e^- , or a neutrino, ν_e , if the interaction is driven by neutral or charged current, respectively*. In both cases the virtual boson carries momentum $q = p - p'$. When the momentum transfer is large enough, the virtual boson acts as a probe of the internal structure of the proton, which is dominated by color-confined strong interactions. Thus, measurements of this family of scattering process are an excellent experimental handle on the behavior of strong nuclear forces and the nature of the elementary degrees of freedom of the hadronic side of the Standard Model.

It is customary to parameterize the scattering using two out of three of the following invariants

$$\text{virtuality } Q^2 = -q^2, \quad (2a)$$

$$\text{Bjorken } x = \frac{Q^2}{2P \cdot q}, \quad (2b)$$

$$\text{and inelasticity } y = \frac{P \cdot q}{P \cdot p}. \quad (2c)$$

The observable Q^2 defines the energy scale of the boson probing the proton structure, while Eq. (2b) defines the lowest fraction of momentum that a struck quark or gluon inside the proton can carry. Finally, Eq. (2c) quantifies the energy loss of the electron. This choice of variables is especially relevant in the neutral current case as it allows to fully characterize the cross-section from measurements of the final state lepton only. Indeed, one of the main goals of the EIC program is a high precision determination of the proton structure and its dependence on Q^2 [6], this motivates theoretical effort in improving the prediction for the same observables.

Beside the inclusive cross-section, we can learn more about the features of the strong interactions, *e.g.* the value of strong coupling α_s or the details of the QCD radiation patterns, by studying directly properties of the ensemble of hadrons emerging in the final state. Event shapes observables are one way to

*While we focus on the case of electron beams here, the described methods are of course likewise available for positron beams

approach this task as they evaluate the geometrical distribution of particles in the final state. Specifically for this work, we consider the 1-jettiness distribution,

$$\tau = \frac{2}{Q^2} \sum_{i \in X} \min(p_i \cdot (xP), p_i \cdot (xP + q)). \quad (3)$$

This is a measure the collimation of hadrons around the direction of the incoming or produced parton and in DIS is equivalent to the thrust event shape [30].

A complementary approach to the above study of the global hadronic final state is the clustering of hadrons into jets. In modern experimental analyses, jets are usually defined in terms of sequential clustering algorithms [31]. For this purpose, we consider three variants from Refs. [32–34], defined by the clustering distance measures for two hadrons p_i, p_j

$$d_{ij}^{k_t} = \min(k_{ti}^2, k_{tj}^2) \frac{\Delta_{ij}^2}{R^2}, \quad d_{iB} = k_{ti}^2, \quad (4a)$$

$$d_{ij}^{\text{anti-}k_t} = \min\left(\frac{1}{k_{ti}^2}, \frac{1}{k_{tj}^2}\right) \frac{\Delta_{ij}^2}{R^2}, \quad d_{iB} = \frac{1}{k_{ti}^2}, \quad (4b)$$

$$d_{ij}^{\text{Centauro}} = \frac{1}{R^2} \left[(f_i - f_j)^2 + 2f_i f_j (1 - \cos \Delta\phi_{ij}) \right] \quad \text{with } f_i = 2\sqrt{1 + \frac{q \cdot p_i}{xP \cdot p_i}}, \quad d_{iB} = 1, \quad (4c)$$

where $\Delta_{ij}^2 = (y_i - y_j)^2 + (\phi_i^2 - \phi_j^2)$ is the distance in the azimuthal plane between the two hadrons and y, ϕ and k_t are the rapidity, azimuthal angle and transverse momentum relative to the beam axis of each hadron, respectively. All quantities here are defined in the Breit frame for our purposes[†]. The parameter R controls the expected average size of the jet. All these tools allow for the characterization of events in terms of leading jet transverse momentum and pseudorapidity, as well as the overall jet multiplicity and invariant masses of di-/tri-jet systems.

Finally, given a definition of jets, one more handle on the behavior of QCD radiation is offered by the internal structure of the jet themselves. Analyses of jet substructure are a tool extensively used at the LHC [35–38]. A common goal is to remove soft radiation at wide angles from the jet axis, which is typically dominated by contamination from sources outside the jet and hadronization corrections. This can be achieved by the so called soft-drop grooming technique [39]. While originally introduced in the context of jets at hadron colliders, and the LHC specifically, it has since been explored in many other contexts such as event shapes at hadron [40] as well as lepton colliders [41, 42], in Higgs decays [43] and for jets measured at lower energy experiments such as RHIC [44]. Here, we consider the application in DIS described in [45] to soft-drop on top of the CENTAURO clustering (see above). Related observables have recently been measured in DIS for the first time [46]. Briefly, this entails first clustering the hadronic ensemble X with the standard algorithm and then step backwards through the jet clustering history. At each branching, if

$$\frac{\min(z_i, z_j)}{z_i + z_j} < z_{\text{cut}}, \quad z_i = \frac{P \cdot p_i}{P \cdot q}, \quad (5)$$

where z_{cut} defines the cut-off parameter for the procedure, the softer subjet is discarded and the procedure continues along the harder branch. The algorithm terminates if either Eq. (5) is not met or there is only one particle left in the jet. After this grooming procedure is completed the surviving particles can be used to compute any hadronic observable. For this work, we will consider the groomed 1-jettiness:

$$\tau_{\text{Gr}} = \frac{2}{Q^2} \sum_{i \in X_{\text{Groomed}}} \min(p_i \cdot (xP), p_i \cdot (xP + q)). \quad (6a)$$

[†]The Breit frame, or brick wall frame, is defined as the frame in which the momentum transfer is

$$q = Q(0, 0, 0, -1),$$

this provides a natural separation hemispheres between the leptonic and hadronic side of DIS at Born level.

3 Event Generation for DIS in SHERPA

For our hadron-level predictions, we use the SHERPA v3 [47] event generator. It provides matrix elements at tree level through the internal generators AMEGIC [48] and COMIX [49]. Virtual corrections for the DIS process are likewise included internally. We use SHERPA’s default CSSHOWER [50] based on Catani–Seymour dipoles [51]. It can be matched to NLO matrix elements using the MC@NLO [52] method. Matrix elements with different multiplicities are combined using the CKKW merging method [53]. Events can be hadronized using the cluster hadronization model [54] as implemented in SHERPA [55, 56] or alternatively the Lund model using an interface to PYTHIA 8 [57]. The events are analyzed using SHERPA’s interface to RIVET [58].

3.1 MEPS@LO, MC@NLO and MEPS@NLO

The automation of matching and merging for DIS in SHERPA has been presented in [12]. Matching to higher order matrix elements is achieved through SHERPA’s implementation of the MC@NLO prescription [59]. Merging in the CKKW method is achieved by applying a jet criterion at the matrix-element level and restricting the available phase space for the parton shower. To maintain the logarithmic accuracy, a backwards clustering has to be performed to dress matrix elements with appropriate Sudakov factors and evaluate α_s at the correct scale. The techniques used in this work are known as MEPS@LO [11] and MEPS@NLO [13, 14], and we refer to the respective publications for the details of the procedures and subtleties related to the use of NLO matrix elements.

In our calculations, we compute single- and di-jet production at NLO and three- and four-jet production at LO, *i.e.*

$$e^- p \rightarrow e^- + 1, 2 j @ \text{NLO} + 3, 4 j @ \text{LO} \quad (7)$$

for neutral-current DIS and

$$e^- p \rightarrow \nu + 1, 2 j @ \text{NLO} + 3, 4 j @ \text{LO} \quad (8)$$

for CC DIS at MEPS@NLO, and analogous simplified processes for MEPS@LO, MC@NLO and LO predictions. In the neutral-current interactions, we treat the light quarks as massless and additionally compute and merge in processes with massive c - and b -quarks at LO. In the parton shower, c and b quarks are likewise treated using massive splitting functions[60]. For the charged-current simulation, we work with 4 massless quarks. The b does not contribute to jet production since we assume a diagonal CKM matrix, and is anyway heavily suppressed by the PDF.

When merging higher-multiplicity matrix elements, each process has to be clustered back to a $2 \rightarrow 2$ configuration. An exemplary diagram which involves all possible clustering steps is shown in Fig. 1. Depending on the hierarchy of the propagators’ momenta, q and k_i , for any given event one can distinguish three different core processes and their corresponding scale μ_{core} :

- (i) virtual photon exchange, *i.e.* $ej \rightarrow ej$, where $\mu_{\text{core}}^2 = Q^2$,
- (ii) interaction of the virtual photon with a QCD parton, *i.e.* $\gamma^* j \rightarrow j_1 j_2$, with $\mu_{\text{core}}^2 = m_{\perp,1} m_{\perp,2}$ defined as the product of the two jet transverse masses $m_{\perp,i} = \sqrt{m_i^2 + p_{\perp,i}^2}$ relative to the beam axis,
- (iii) pure QCD channels, *i.e.* $jj \rightarrow jj$, where $\mu_{\text{core}}^2 = -\frac{1}{\sqrt{2}} (s^{-1} + t^{-1} + u^{-1})^{-1}$ is a scaled harmonic mean of the Mandelstam variables s, t, u .

The factorization and shower starting scales are then set to the core scale, *i.e.* $\mu_{\text{F}} = \mu_{\text{R}} = \mu_{\text{Q}} = \mu_{\text{core}}$. For higher multiplicities, the renormalization scale is determined according to the clustering algorithm [11] with μ_{core} as scale of the core $2 \rightarrow 2$ process.

The merging scale Q_{cut} , *i.e.* the separation of the phase space into a region filled by additional legs in the matrix elements instead of the parton shower, is dynamically given by

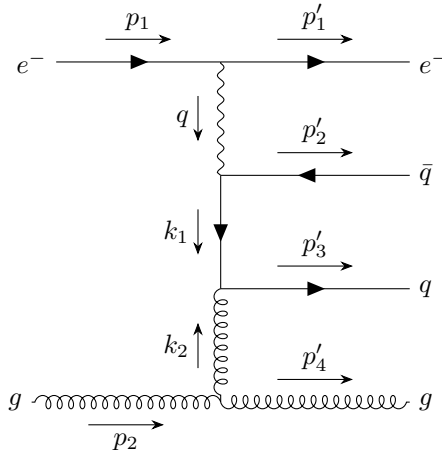


Figure 1: Sketch of an example Feynman diagram with three final-state partons in DIS. Depending on the hierarchy of the internal momenta, the event is clustered back to an underlying $2 \rightarrow 2$ core process. Only if $q^2 \gg k_1^2, k_2^2$ holds, is the core process DIS-like.

$$Q_{\text{cut}} = \frac{\bar{Q}_{\text{cut}}}{\sqrt{1 + \frac{\bar{Q}_{\text{cut}}^2}{S_{\text{DIS}} Q^2}}} \quad (9)$$

using $\bar{Q}_{\text{cut}} = 25 \text{ GeV}$ and $S_{\text{DIS}} = 0.4$. The former avoids unnecessary multi-leg matrix elements, while the latter ensures a decrease of the merging scale towards smaller virtualities, therefore improving the description in this region.

For the parton densities, we use the NNPDF30_nlo_as_0118 set [61] using LHAPDF [62]. LHAPDF is also used for the α_s evolution, ensuring consistency with the PDF set and in particular implying $\alpha_s(M_Z) = 0.118$.

3.2 Systematic uncertainties of event generation in DIS

A systematic assessment of theoretical uncertainties is crucial in high-energy phenomenology due to increasing precision in calculations, simulations, and experiments. For a Monte Carlo event generator like SHERPA, two primary sources of uncertainties exist: theoretical uncertainty from truncation of perturbative series expansion, and uncertainty in modeling and tuning parton fragmentation and hadronization due to the lack of a first-principle solution for long-range QCD interactions.

The first source encompasses several perturbative ingredients of the calculation, i.e. the evaluation of hard matrix elements at various multiplicities in merged samples, as well as parton shower evolution. We follow the established approach of estimating the size of missing higher perturbative orders by examining the residual dependence of resulting observables on the renormalization and factorization scales. We note though that this approach has severe limitations and especially in the context of even higher order calculations it might be appropriate to investigate other sources of uncertainty [63–67]. Here, we perform 7-point variations around a central choice $(\mu_{F,0}, \mu_{R,0})$, considering all ratios

$$(\mu_F/\mu_{F,0}, \mu_R/\mu_{R,0}) \in \{(1, 1), (1, 2), (1, 0.5), (2, 1), (0.5, 1), (0.5, 0.5), (2, 2)\}. \quad (10)$$

We apply these variations in the matrix-element calculation and the parton-shower evolution simultaneously. Ultimately, we build our estimate of the perturbative uncertainty from the envelope of all scale choices. It is worth stressing that, in this procedure, we are varying scales appearing in the parton shower, which affects the evaluation of α_s and the PDF ratios. Providing more extensive parton shower

uncertainties is an open topic of research, complicated by the fact that parton showers include significant subleading contributions [68]. We here stay restricted to the traditional scale variations. SHERPA performs this operation on-the-fly [69], which significantly reduces computing costs compared to running separate simulations for each scale setting.

The second source of uncertainty relates to the non-perturbative modeling of parton fragmentation into hadrons. These uncertainties arise from phenomenological models rather than first-principle calculations, leading to a significant model dependence. To evaluate fragmentation corrections, we use SHERPA’s internal cluster hadronization model [56] and the Lund String model via an interface to PYTHIA 8 [57]. The symmetrized difference between these two models is taken as the uncertainty[‡], using the cluster model as the central value.

Another aspect of non-perturbative modeling involves tuning model parameters to data. We use the replica tunes from Ref. [70] to estimate uncertainties related to the tuning of final state fragmentation parameters and the variations from Ref. [71] for parameters governing cluster decays involving beam remnants. This introduces two sets of variations within the cluster model itself, for which we take the respective envelopes for each histogram as the related uncertainty. As a result, three sources of non-perturbative uncertainty arise: model choice, final state fragmentation tune, and beam fragmentation tune. Arguably the different sources of uncertainty should be combined. We however find that usually only one, in most cases the model choice, dominates the overall uncertainty. We hence only show the three sources independently, without a combination.

Since estimating non-perturbative uncertainties requires independent Monte Carlo runs for each parameter set, and for both models, performing this study for the full MEPS@NLO, MEPS@LO and MC@NLO setups is infeasible. Instead, we derive the relative uncertainty based on parton showered leading-order matrix elements merged together in the MEPS@LO approach. A merged approach is still beneficial to ensure sufficient phase-space coverage. In the following we only treat the results of two tunes or models as different if we can statistically distinguish them at a level of 3 standard deviations, and otherwise indicate the statistical error that serves as an upper bound on the uncertainty.

We make no attempt to directly apply this uncertainty to higher- or lower-precision simulations, though one could envision a procedure based on transfer matrices introduced in Ref. [72]. Additionally, we do not combine non-perturbative and perturbative uncertainty estimates but rather focus on comparing their relative sizes in the following analysis.

4 Event Generation for HERA and MEPS@NLO in charged current DIS

The SHERPA framework has been extensively used in the past to describe neutral current DIS at HERA, see for example Ref. [12]. Early versions of SHERPA 3 were also used in a variety of recent event shape and jet analyses by the H1 collaboration [74–76, 46, 77], usually finding satisfactory agreement with the data. A MEPS@NLO setup similar to the one used here was compared to resummed calculations for event shapes in Refs. [71, 78]. The latter also determined part of the current tune of non-perturbative parameters. With this, we consider the framework and MEPS@NLO to be sufficiently validated in neutral current DIS, and we focus in the following on the first detailed comparison to CC data from HERA.

We compare our Monte Carlo setups against multi-jet cross-sections in CC DIS measured by the ZEUS collaboration [73]. We consider beams of electrons at 27.5 GeV and protons at 920 GeV. To model the proton contents, we use the NNPDF30_nlo_as_0118 set as discussed in Sec. 3.1.

A caveat for CC DIS is that, in contrast to NC DIS, it is impossible to use the final state neutrino to reconstruct q . Therefore, the measurements of Eqs. (2) involve the reconstruction of the full hadronic final state under the condition of large missing p_t from the invisible high-energy neutrino. The details of this procedure are discussed in Refs. [73, 79]. At the hadronic simulation level, we ignore this complication

[‡]Note this procedure can in principle result in uncertainties covering negative (differential) cross-sections. These are clearly unphysical and we cut off the envelope at zero.

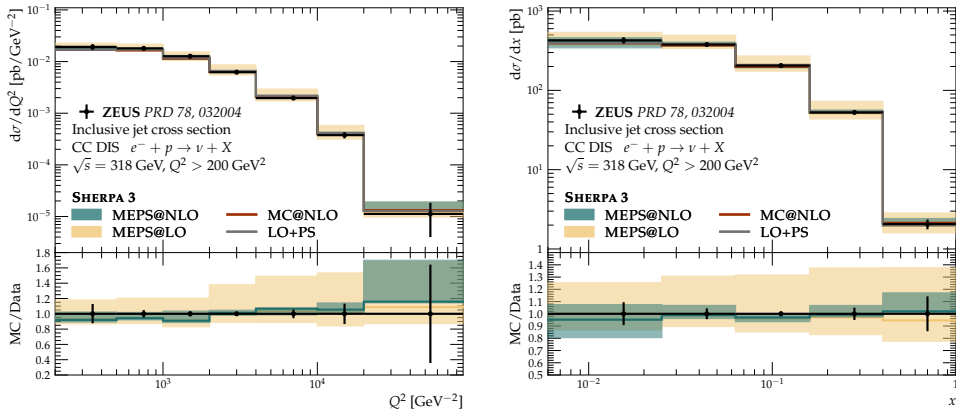


Figure 2: Differential distributions for Q^2 and x at LO, MC@NLO, MEPS@LO and MEPS@NLO in inclusive CC DIS at the HERA. The lower panels show the ratio between data and the merged MEPS@LO and MEPS@NLO predictions, while we omit the ratio for the LO and MC@NLO simulations for clarity. Experimental data points are from Ref. [73].

and consider the recoil neutrino as known for the determination of Q^2 , x and y . In the analysis, events are selected following the experimental phase space cuts:

$$Q^2 > 200 \text{ GeV}^2, \quad y < 0.9, \quad N_{\text{jets}} \geq 1, \quad E_{T,\text{leading jet}} > 14 \text{ GeV}, \quad E_{T,\text{any jet}} > 5 \text{ GeV}. \quad (11)$$

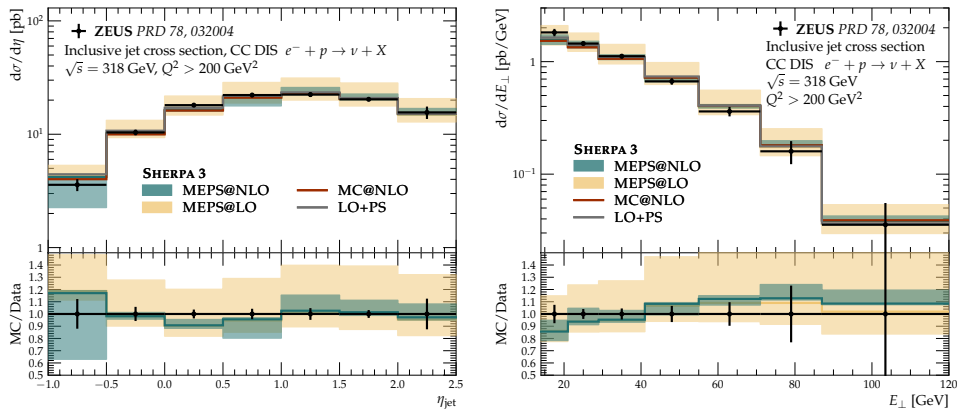


Figure 3: Differential distributions for η_{jet} and $E_{T,\text{jet}}$ at LO, MC@NLO, MEPS@LO and MEPS@NLO in inclusive CC DIS at the HERA. The lower panels show the ratio between data and the merged MEPS@LO and MEPS@NLO predictions, while we omit the ratio for the LO and MC@NLO simulations for clarity. Experimental data points are from Ref. [73].

In Figs. 2 and 3, we reproduce the differential cross-sections for inclusive-jet production as functions of Q^2 , x , and leading-jet η and E_{\perp} . Due to the relatively large Q^2 requirement, higher-order corrections are rather small, and we find the simulations at all accuracy levels to be consistent with each other and with the data. In particular, the lack of a sizable shift between the LO and MEPS@NLO predictions can be attributed to the high Q^2 cut. This requirement restricts the phase space to regions where merging effects remain small. The lower panels, we show the ratio of the merged simulations to data. Since the central values for all Monte Carlo accuracies are very consistent, we do not show ratios for the LO and

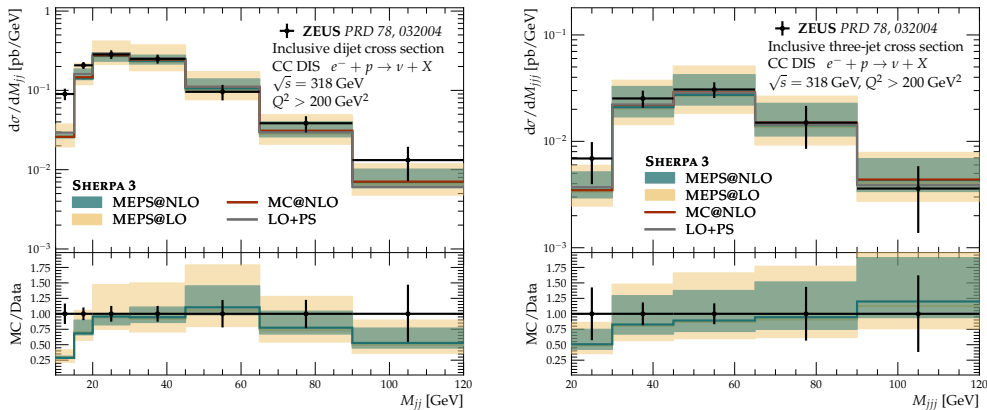


Figure 4: Multijet distributions differential in the mass of the two (left) or three (right) leading jets at LO, MC@NLO, MEPS@LO and MEPS@NLO in inclusive CC DIS at the HERA. The lower panels show the ratio between data and the merged MEPS@LO and MEPS@NLO predictions, while we omit the ratio for the LO and MC@NLO simulations for clarity. Experimental data points are from Ref. [73].

MC@NLO runs to increase legibility. For the two remaining runs, we also plot the band obtained from scale variations. Notably, while the central value is almost unchanged when going from MEPS@LO to MEPS@NLO, the scale dependence is reduced dramatically. This leads to some visible systematic trend of the MEPS@NLO simulation against data, especially in the transverse energy distribution, but the data is not precise enough there for a definite conclusion.

In Fig. 4, the dijet and three-jet invariant mass cross-sections are presented. The different Monte Carlo samples are again very consistent with each other. For the dijet mass, some deviations appear for very small and very large masses, although only those at small masses have any statistical significance. In the range $20 \text{ GeV} < M_{jj} < 120 \text{ GeV}$, the Monte Carlo predictions are consistent with the data. In the three-jet mass case, prediction and data are consistent over the full measured range, albeit admittedly with significantly larger uncertainties on the data. The scale variations are reduced in both cases, although they remain sizable in the three-jet case.

Overall, we find the agreement between Monte Carlo simulation and data satisfactory for CC DIS as well. In the future it would be interesting to study further analyses performed by the HERA collaborations in this process. Unfortunately, the availability of automated analyses in RIVET is limited in this case.

5 Event generation for the EIC and its systematic uncertainties

In this section, we present predictions for DIS at the EIC for both neutral and charged current interactions. As outlined in Sec. 2, we analyze a combination of global observables, including the Q^2 , y , and x distributions. For neutral current interactions, we additionally provide results for the transverse momentum of the recoil lepton, while for charged current interactions, we examine the missing transverse momentum.

Furthermore, we compare jet properties obtained using the k_t , anti- k_t , and CENAURO clustering algorithms, highlighting differences in jet multiplicities and leading jet transverse momentum. Finally, to probe the hadronic final state, we study the 1-jettiness distribution, presented in slices of Q^2 and x .

These observables are evaluated using all Monte Carlo configurations discussed in Sec. 3.1, allowing for a detailed comparison of the effects of matching, merging, and higher-order corrections. Our main goal is to evaluate the role of MEPS@NLO and in what phase space it is to be preferred to the other configurations. We also estimate hadronization uncertainties as explained in Sec. 3.2.

For both neutral and charged current DIS, we assume energies of 18 GeV and 275 GeV for the lepton

and proton beams respectively; this corresponds to the high-luminosity configuration of the EIC. We do not consider any polarization of the beams.

To arrive at realistic predictions, we discard particles outside an assumed detector acceptance of $|\eta| > 4$ during the analysis and apply a cut on the inelasticity, keeping the interval $0.2 < y < 0.9$. Jets are clustered with a minimal transverse momentum of 5 GeV and a jet radius of $R = 1$. While we follow the setup of tradition studies like Ref. [16], the CENTAURO algorithm presents new advantageous options that should be explored in dedicated studies [80].

5.1 Neutral Current

We consider the neutral current setup first. In this case, we place a small virtuality cut, $Q^2 > 6 \text{ GeV}^2$. We present the global DIS observables Q^2 , x , y and p_T^{lep} in Fig. 5. For Q^2 and x , the merged calculations exhibit distinct behavior from the matched MC@NLO approach. In the Q^2 distribution (top left), we observe that for $Q^2 < 20 \text{ GeV}^2$, the MEPS@NLO prediction exceeds LO and MC@NLO of up to 30%, while showing a more modest 10% enhancement over MEPS@LO. This enhancement exceeds the scale uncertainty bands between MEPS@NLO and MC@NLO but remains within the MEPS@LO uncertainties. The predictions converge in the intermediate region $20 \text{ GeV}^2 \leq Q^2 \leq 5 \cdot 10^3 \text{ GeV}^2$. At higher virtualities ($Q^2 > 5 \cdot 10^3 \text{ GeV}^2$), we observe a systematic 10% deficit in the LO and MEPS@LO predictions relative to the NLO-accurate calculations, showing the importance of the virtual $\mathcal{O}(\alpha_s)$ corrections in this regime.

Similar patterns can be seen in the x and p_T^{lep} distributions (top and bottom right). Multi-jet merging effects dominate at $x < 1.5 \cdot 10^{-3}$ ($p_T^{\text{lep}} < 5 \text{ GeV}$), while NLO matching becomes crucial at $x > 0.7$ ($p_T^{\text{lep}} > 65 \text{ GeV}$). The MEPS@NLO calculation shows reduced scale uncertainties compared to MEPS@LO in the low- x and low- p_T^{lep} regions. It also shows smaller uncertainties than MC@NLO in the intermediate ranges of around $Q^2 \approx 10^2 \text{ GeV}^2$ and $x \approx 10^{-2}$ as a consequence of calculating the $2 \rightarrow 3$ process to NLO. The inelasticity distribution (bottom left) reveals good agreement between MEPS@NLO and MEPS@LO across the full range, while LO and MC@NLO predictions are uniformly suppressed by approximately 25%, though this deviation remains within the combined scale uncertainty bands.

The observations above are in line with the general trends for example at HERA energies. We do not display any hadronic uncertainty as these observables are not affected within the models we consider.

Figure 6 presents the jet multiplicity and leading jet transverse momentum distributions for three different clustering algorithms. While MEPS@NLO and MEPS@LO predictions show good concordance, both MC@NLO and LO calculations yield systematically lower rates. Despite reduced scale uncertainties in MEPS@NLO compared to MEPS@LO, both merged calculations exhibit significant scale variations, reflecting the LO accuracy of higher-multiplicity configurations that dominate the low- Q^2 regime and that contribute significantly in these observables. It is also worth noting that the CENTAURO clustering algorithm leads to smaller higher-order corrections in this analysis. Indeed, the LO simulation is unable to fill the whole phase space. For the k_t and anti- k_t , the MC@NLO sample is still off, compared to the merged ones, by a K -factor of about 1.5 for the low- p_T region. Conversely, the CENTAURO algorithm shows much smaller K -factors, in fact only a factor of 1.2 for the low- p_T region with respect to the MEPS@NLO prediction.

Hadronization uncertainties are generally smaller than the perturbative uncertainties and, as one might have expected, are largest for small p_T (up to 5%) and for large jet multiplicities (1 – 2%). In the latter, we find that only a variation of the fragmentation model induces a significant effect, while replica tunes within the cluster model are negligible. Instead, in the p_T spectrum, fragmentation model uncertainty is still the largest non-perturbative contribution for the anti- k_t and k_t jets, while variations from replica tunes are larger than model ones for CENTAURO jets, although both are especially small. Beyond small values of p_T , the difference between hadronization models becomes unresolvable within the accumulated statistics. Instead, the combined statistical uncertainty from the two models is taken as an overestimate. These values are still comparable or subdominant to the perturbative uncertainties in the same part of the spectrum.

We finally consider 1-jettiness, an event shape variable that is sensitive to the underlying parton dynamics and can be used, e.g., for global fits of the strong coupling constant α_s [81]. In Ref. [82],

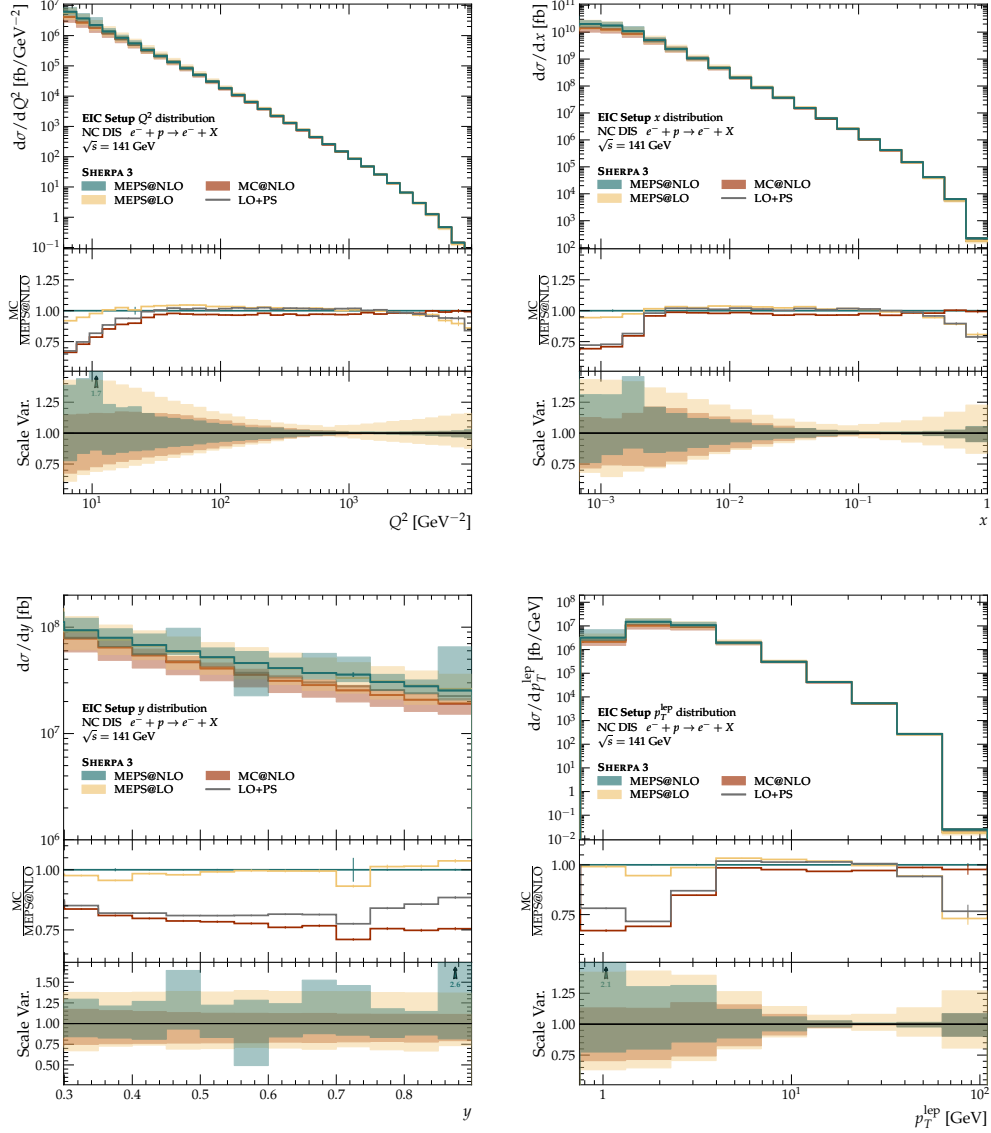


Figure 5: Differential distributions for Q^2 (top left), x (top right), y (bottom left) and lepton transverse momentum p_T^{lep} (bottom right) in NC DIS at the EIC, comparing LO+PS, MC@NLO, MEPS@LO and MEPS@NLO predictions. The main panels show results with scale variation uncertainties for all but the LO+PS calculation. The first ratio panel displays the relative deviation from MEPS@NLO to highlight merging effects. The second ratio shows the relative scale uncertainties.

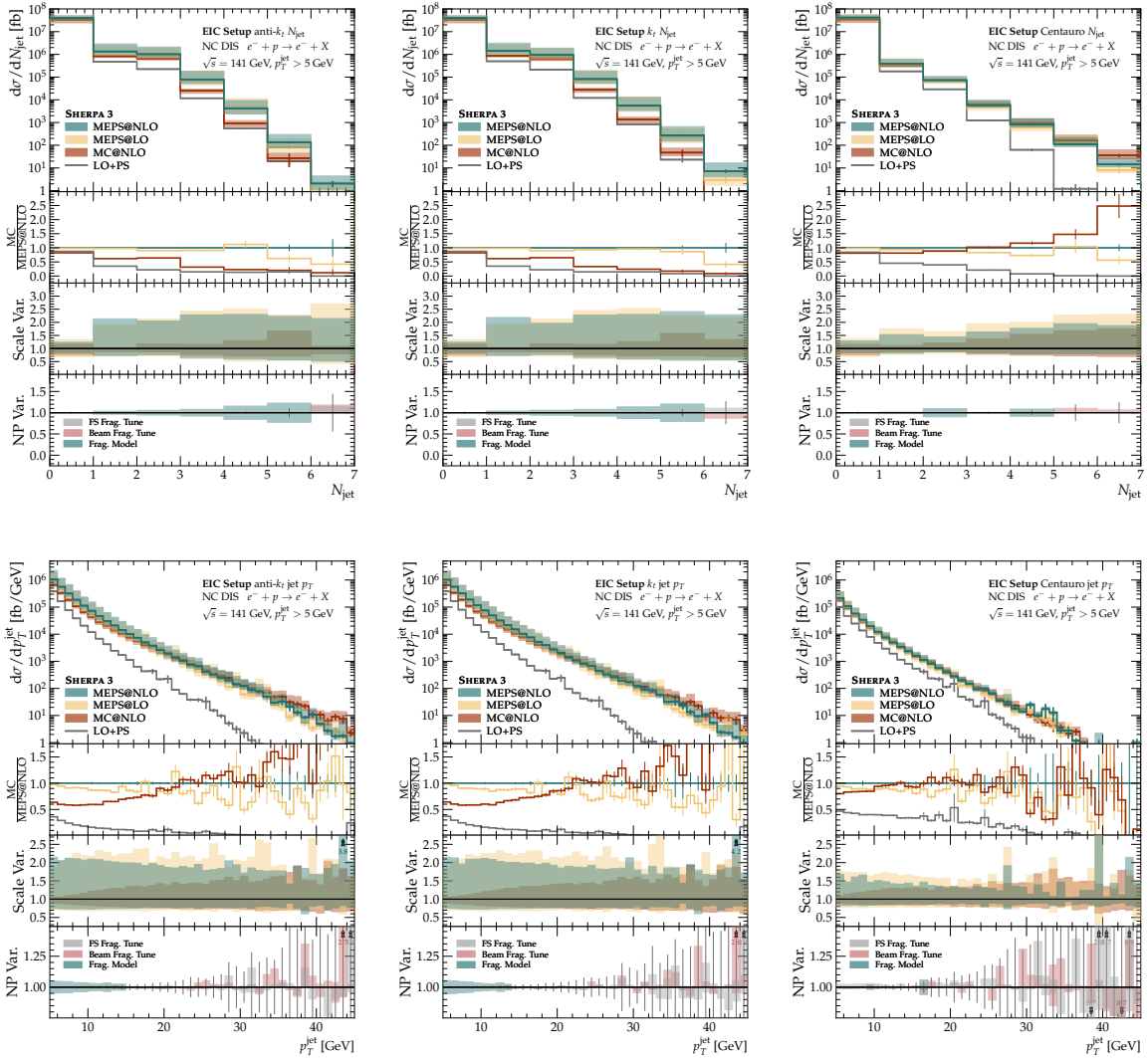


Figure 6: Jet multiplicity N_{jet} (top row) and leading jet transverse momentum p_T^{jet} (bottom row) distributions for anti- k_t (left), k_t (middle) and CENAURO (right) jet algorithms in NC DIS at the EIC. The bottom ratios in each row indicate, from top to bottom, the ratio of each prediction to the MEPS@NLO one, the uncertainty from scale variations and the uncertainty from non-perturbative model and tuning variations. The error bars in the lowest panel indicate the statistical uncertainty of the difference between cluster and string model.

predictions of 1-jettiness at the EIC were computed with NNLO+N³LL accuracy. Here, we present in Figure 7 an overview of the 1-jettiness τ across bins of x (left to right) and Q^2 (top to bottom). For the sake of presentation we omit the ratio panels here, the full plots can be found in the appendix. Overall, the shape of the distributions agree well between the different configurations. Similar to the behavior at the recent H1 measurement [76], we observe that the high- Q^2 has a pronounced peak at small τ values, while the low- Q^2 distributions tend to higher values, which underlines the importance of high-multiplicity matrix elements in the latter regime.

For a more thorough discussion, we show the full breakdown of ratios and uncertainties in Fig. 8 for three different x regions in the $10 < Q^2/\text{GeV}^2 < 31.6$ range. Plots for the other x - Q^2 ranges in Fig. 7 can be found in App. A.1. We observe that the non-perturbative uncertainties are non-negligible for small τ

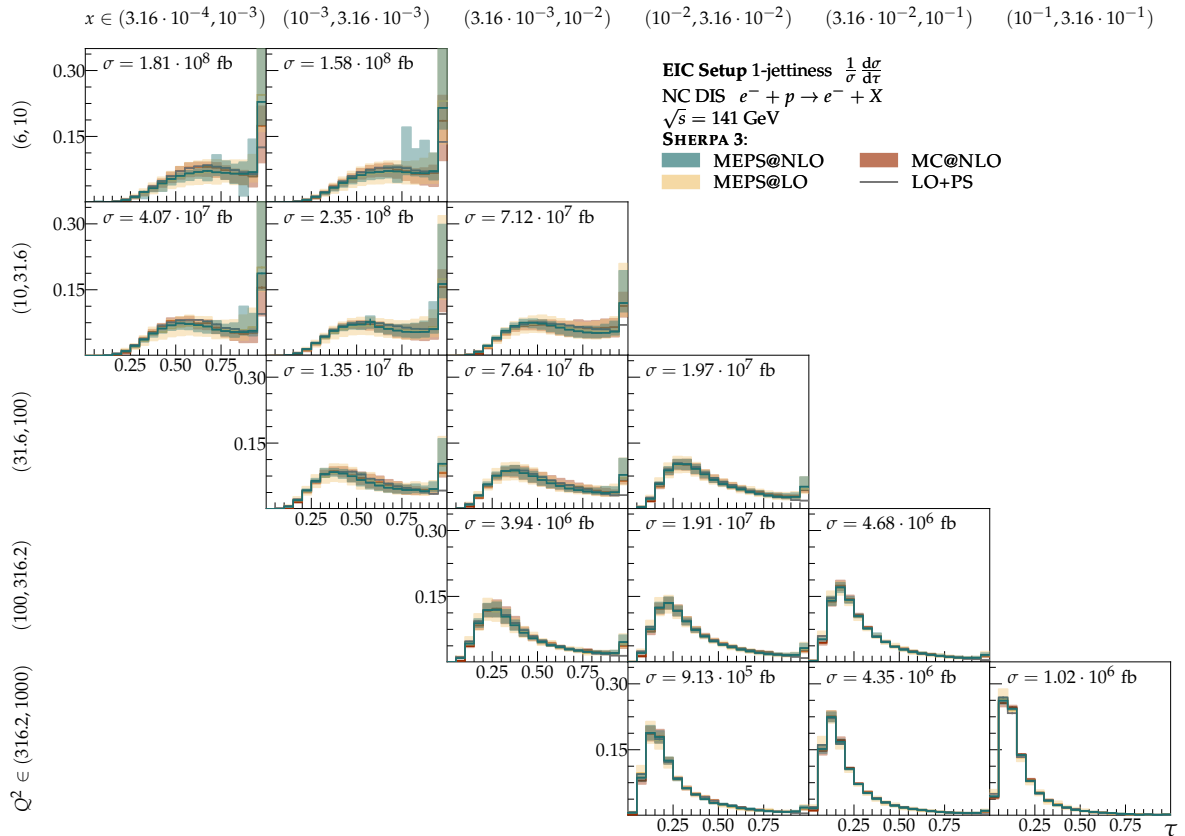


Figure 7: Differential distributions of 1-jettiness τ in different bins of Q^2 and x in NC DIS at the EIC. The total MEPS@NLO cross-section for each x - Q^2 bin is reported on top of the corresponding plot.

values and of similar size as the MC@NLO and MEPS@NLO scale uncertainties in that region. The same qualitative behavior is visible in both the tuning variations and the difference between string and cluster models, while the latter are significantly larger. This is the case for both tuning uncertainties and variations of the hadronization model, where the latter are dominating. For larger values of 1-jettiness, either of the considered non-perturbative uncertainties are negligible, consistent with the observations in [71]. Furthermore, the non-perturbative uncertainties are—unsurprisingly—largest for small values of Q^2 and x . The shape of the distributions at small Q^2 underlines the importance of multi-parton topologies in this region.

At last, in Fig. 9 we report the 1-jettiness event shape after applying the soft-drop to CENTAURO jets. We consider three values of the grooming cut from $z_{\text{cut}} \in (0.05, 0.1, 0.2)$, while remaining inclusive in Q^2 and x . As expected from the removal of soft and low scale radiation, the size of non-perturbative uncertainties is significantly reduced compared to the ungroomed 1-jettiness and does not exhibit strong dependence on z_{cut} . With respect to the MEPS@NLO, the MEPS@LO configuration behaves consistently up to $\tau_{\text{Gr}} < 0.5$. Conversely, the MC@NLO and LO+PS ones are suppressed by a factor 10%. These deviations are still small compared to scale variations, which are reduced switching from MEPS@LO to MEPS@NLO up to $\tau_{\text{Gr}} < 0.8$. Moreover, MEPS@NLO scale uncertainties are generally larger than MC@NLO ones, reinforcing the idea in the low- Q^2 regime LO contributions from higher-multiplicity events provide a large correction.

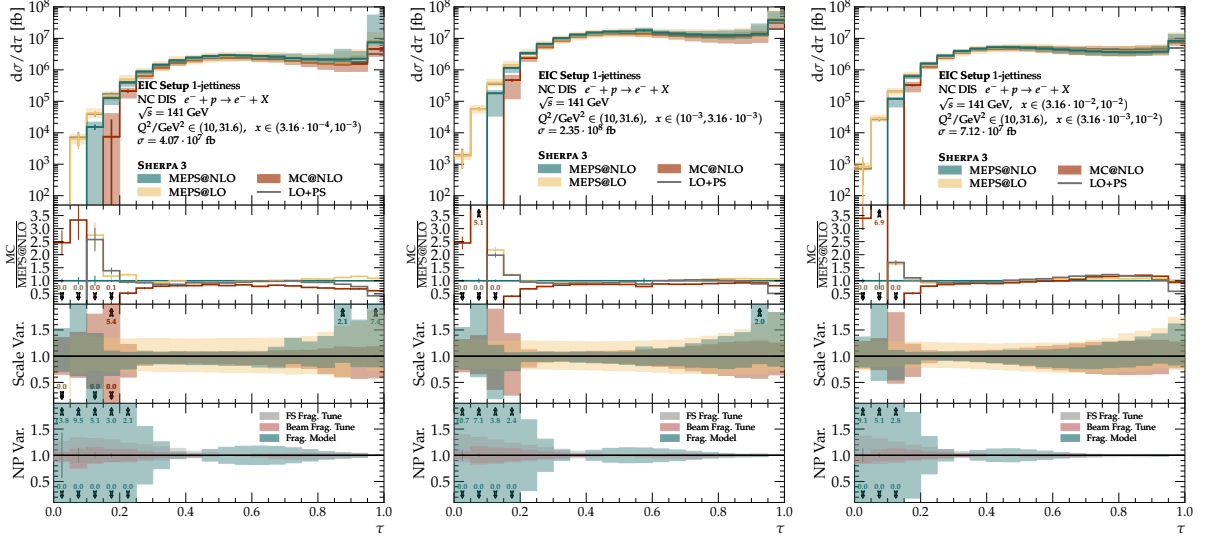


Figure 8: Differential distributions of 1-jettiness τ in a fixed slice of Q^2 and different bins of x in NC DIS at the EIC. The bottom ratios in each row indicate, from top to bottom, the ratio of each prediction to the MEPS@NLO one, the uncertainty from scale variations and the uncertainty from non-perturbative model and tuning variations. The error bars in the lowest panel indicate the statistical uncertainty of the difference between cluster and string model.

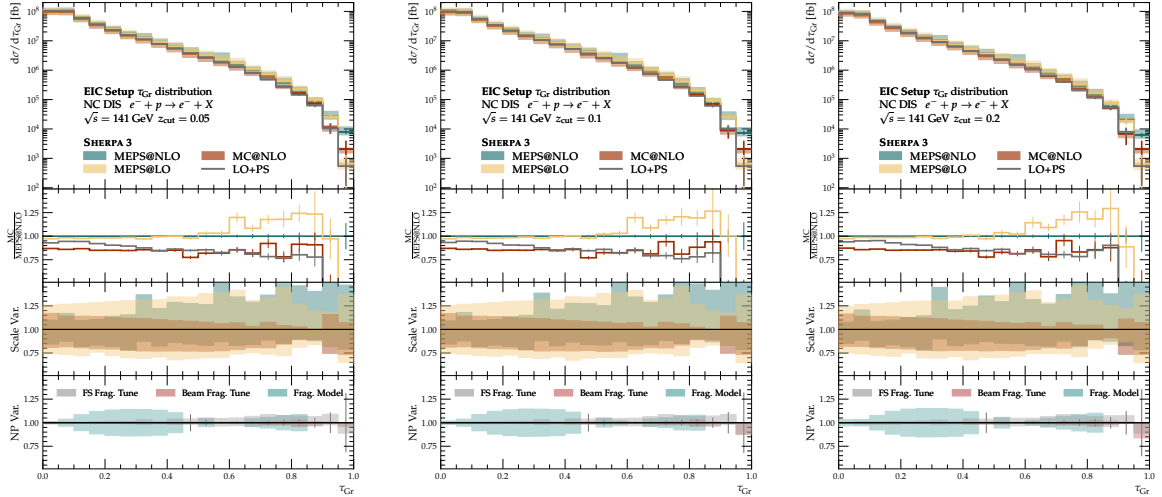


Figure 9: Groomed 1-jettiness in NC DIS at the EIC. From left to right the soft drop cut z_{cut} is 0.05, 0.1 and 0.2. The bottom ratios in each row indicate, from top to bottom, the ratio of each prediction to the MEPS@NLO one, the uncertainty from scale variations and the uncertainty from non-perturbative model and tuning variations. The error bars in the lowest panel indicate the statistical uncertainty of the difference between cluster and string model.

5.2 Charged Current

For the analysis of CC events, we use the same setup as for neutral current events, but we increase the virtuality cut to $Q^2 > 10 \text{ GeV}^2$. This is to account for the experimentally difficult extraction of the correct event kinematics.

We again start our discussion with the global observables, Q^2 , x , y and missing p_T in Figs. 10 and 11. While the inelasticity does not exhibit large differences between the different calculations, we observe rather large corrections for the virtuality and the Bjorken- x distributions. The LO and MC@NLO predictions agree well with each other within the uncertainties, however the merged setups receive large corrections towards decreasing Q^2 , x and missing p_T . This trend starts at values of 10^3 GeV^2 and 10^{-1} , respectively, and reach up to almost a factor of 2 for the lowest Q^2 and x values. With respect to each other the MEPS@LO and MEPS@NLO agree well, the uncertainties are significantly reduced in the latter, as already observed before. Naturally, the MEPS@NLO shows smaller uncertainties than the MEPS@LO and comparable ones to the MC@NLO at high values for the three observables. As multi-jet events dominate at low Q^2 and these events are only computed at LO, the MEPS@NLO shows larger uncertainties than MC@NLO there. Non-perturbative uncertainties were negligible for these observable as they are measured by means of the lepton kinematics and are hence not affected by hadronization.

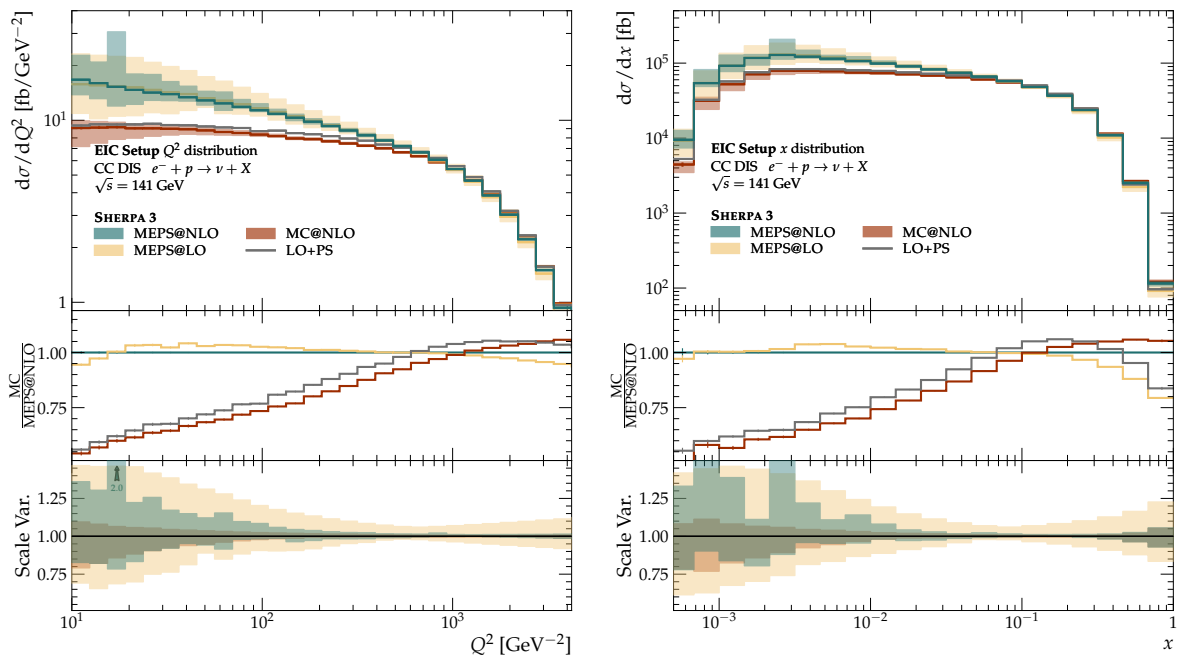


Figure 10: Differential distributions for Q^2 and x in Charged Current DIS at the EIC, comparing LO+PS, MC@NLO, MEPS@LO and MEPS@NLO predictions. The main panels show results with scale variation uncertainties for all but the LO+PS calculation. The first ratio panel displays the relative deviation from MEPS@NLO to highlight merging effects. The second ratio shows the relative scale uncertainties, while the third presents the breakdown of hadronization uncertainties as detailed in Sec. 3.2.

In Fig. 12, we study the three different jet algorithms in terms of jet multiplicity and leading jet transverse momentum. In the latter, and unlike to the neutral current case, there are no corrections with respect to the LO calculation in the low- p_T region for neither of the clustering algorithms. At high p_T the simulation at LO accuracy yields a slightly lower cross-section by about 50% compared to the MEPS@NLO result while the other calculations agree with each other. Hence, we can assume that the large corrections that can be seen in Q^2 and x are driven by small- p_T jets, which are removed by the p_T cut. Seeing that already MC@NLO does not show large differences to the merged setups, we conclude

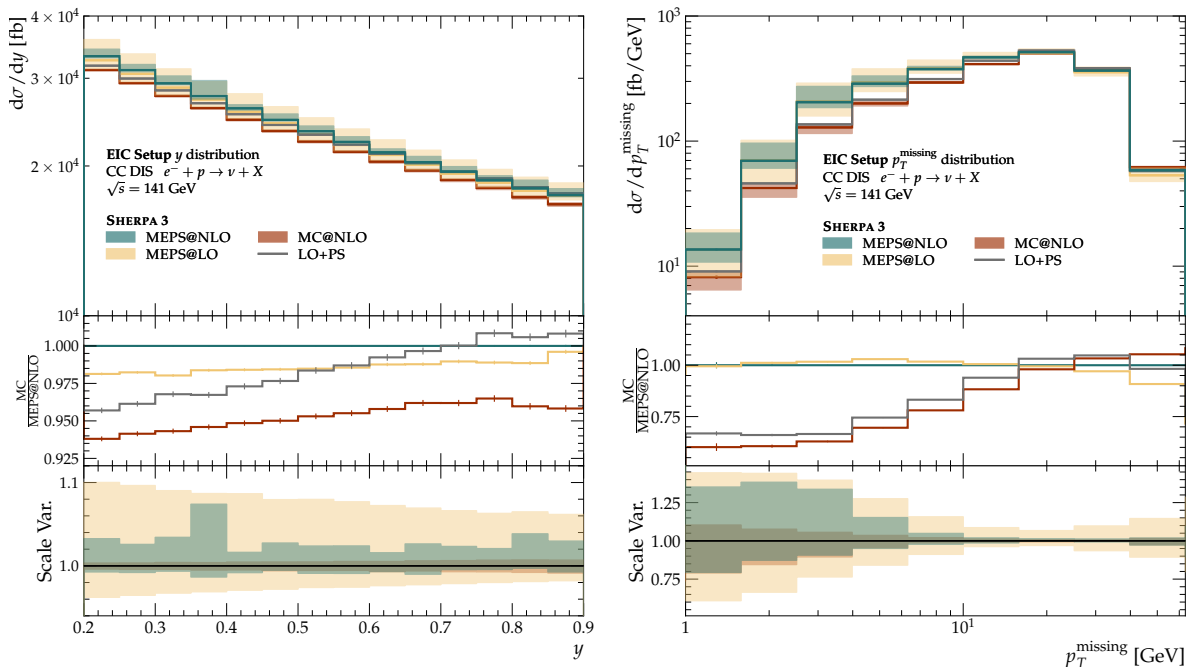


Figure 11: Differential distributions for y and p_T^{missing} in Charged Current DIS at the EIC, comparing LO+PS, MC@NLO, MEPS@LO, and MEPS@NLO. Main panels show scale variation uncertainties (excluding LO+PS). Ratio panels display merging effects and scale uncertainties.

that for jet observables with the used p_T cut of 5 GeV, already the real correction of the Born process captures any corrections in this part of the phase space. As a consequence, the scale uncertainties of the MC@NLO and the MEPS@NLO do not differ as much as in the neutral-current case before. As in the NC case, non-perturbative uncertainties are generally smaller than perturbative ones and affect significantly only the high-multiplicity and low- p_T regions. At most, they account for a relative $\sim 5\%$ correction, which matches the one induced by scale variations only at very low p_T for all jet algorithms considered. Fragmentation model uncertainty is the dominant contribution, while replica tunes within the cluster model do not generate an observable effect within statistical fluctuations.

Analogously to before, we show the 1-jettiness in bins of Q^2 and x in Fig. 13 without ratio plots for clarity and for the range $31.6 < Q^2/\text{GeV}^2 < 100$ in three x ranges including ratio plots in Fig. 14. Note that we pick a different Q^2 slice with respect to the NC case, as the total cross-section in the lower slice is smaller. Plots for the remaining x - Q^2 ranges can again be found in App. A.2. Overall, we see similar changes in the shape when going from small to large virtualities. As the calculation of the 1-jettiness operates inclusively, *i.e.* without a jet cut, we can observe large corrections on the cross-section for low Q^2 by merging additional legs. With regard to the hadronization, we also see the same pattern as before, *i.e.* only the peak is affected and the phase space region of small values of x and Q^2 has larger uncertainties. It is only in these regions that the perturbative and the non-perturbative uncertainties are of comparable size. While 1-jettiness is only an example, this suggests that global analyses of charged-current events at the EIC need higher order corrections for the small virtualities. Depending on the observable, a thorough understanding of non-perturbative effects will also be necessary.

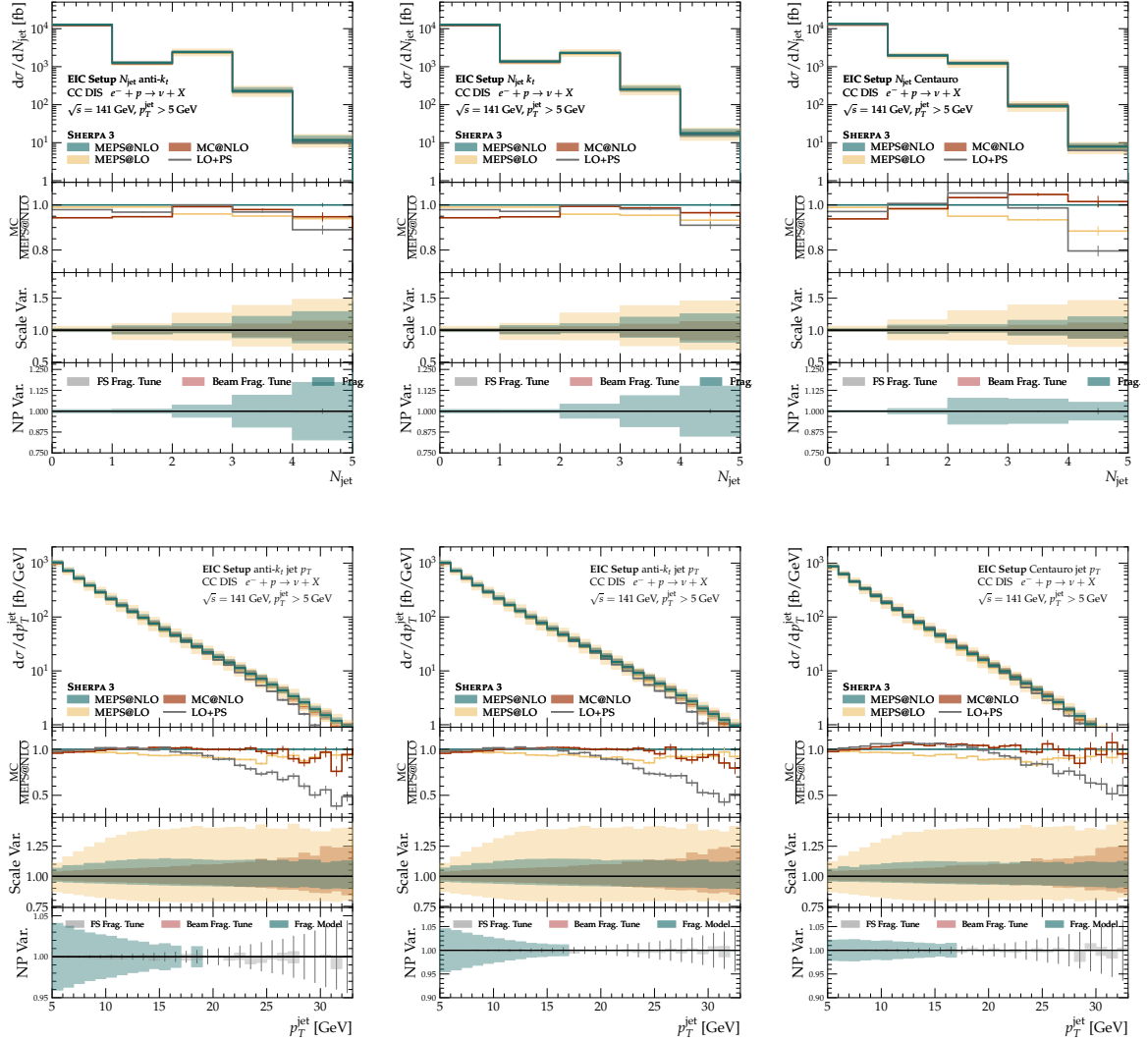


Figure 12: Jet multiplicity N_{jet} (top row) and leading jet transverse momentum p_T^{jet} (bottom row) distributions for anti- k_t (left), k_t (middle) and CENTAURO (right) jet algorithms in CC DIS at the EIC. The bottom ratios in each row indicate, from top to bottom, the ratio of each prediction to the MEPS@NLO one, the uncertainty from scale variations and the uncertainty from non-perturbative model and tuning variations. The error bars in the lowest panel indicate the statistical uncertainty of the difference between cluster and string model.

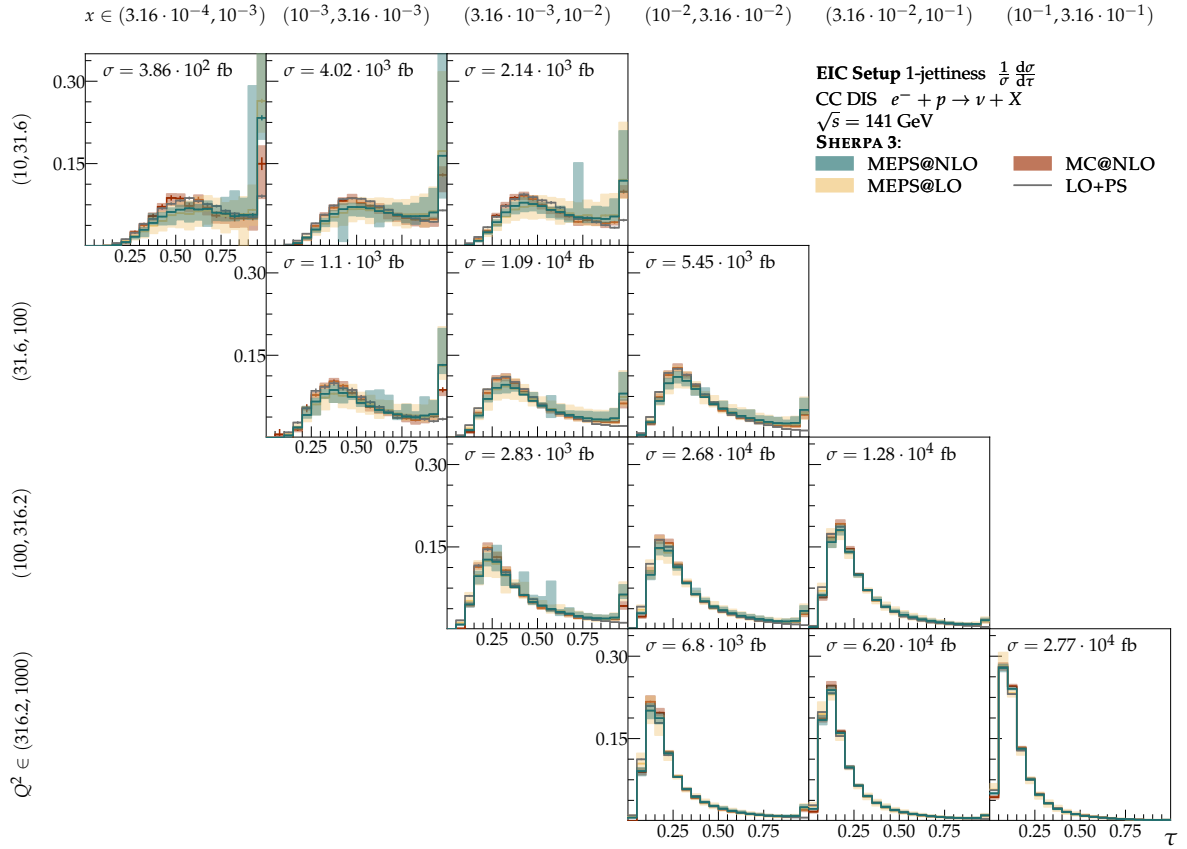


Figure 13: Differential distributions of 1-jettiness τ in different bins of Q^2 and x in CC DIS at the EIC. The total MEPS@NLO cross-section for each x - Q^2 bin is reported on top of the corresponding plot.

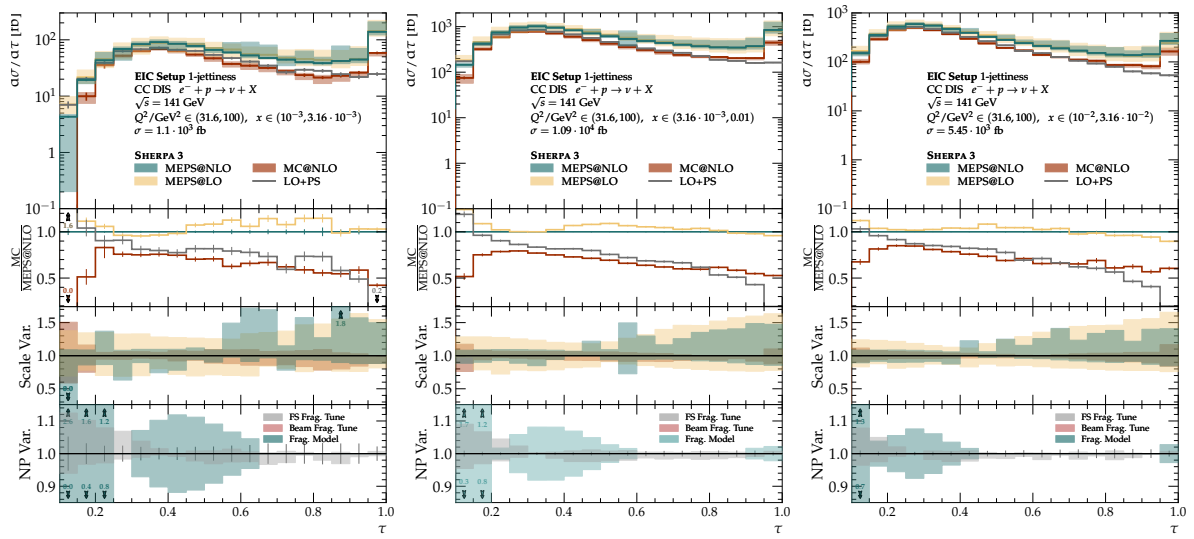


Figure 14: Differential distributions of 1-jettiness τ in a fixed slice of Q^2 and different bins of x in Charged Current DIS at the EIC. The bottom ratios in each row indicate, from top to bottom, the ratio of each prediction to the MEPS@NLO one, the uncertainty from scale variations and the uncertainty from non-perturbative model and tuning variations. The error bars in the lowest panel indicate the statistical uncertainty of the difference between cluster and string model.

6 Conclusion

In this work we presented the first predictions at MEPS@NLO precision for both neutral and charged current DIS at the EIC. Producing full hadron-level predictions, we contrasted perturbative and non-perturbative uncertainties and identified regions where higher-order corrections will be necessary. To this end, we used the multi-jet merging capabilities of the SHERPA event generator, which lead to non-negligible corrections in the cross-sections compared to LO. In the analysis we focused on global DIS observables, jet multiplicities and transverse momenta in the Breit frame and 1-jettiness distributions. While estimating the perturbative higher order uncertainties with 7-point scale variations we examined the non-perturbative uncertainties associated with the fragmentation modeling by means of replica tunes of the hadronization and the uncertainties associated with the choice of non-perturbative model.

We found that the merging of additional legs in the matrix-element in the MEPS@LO and MEPS@NLO schemes, respectively, captures large corrections of up to factor 2 in the low Q^2 and x phase space. The virtual corrections lead to an observable effect on the cross-section, especially at high Q^2 and x . Comparing the k_t , anti- k_t and CENGAURO jet algorithms, we observed very large K -factors for the two former, but only a small K -factor for the latter. We assume this to be a consequence of the CENGAURO algorithm being better at clustering back to a Born kinematics, whereas only higher order corrections contribute for k_t -type algorithms in the Breit frame.

We then studied 1-jettiness as an example for a global event-shape observable, enabling among others the extraction of the strong coupling in measurements at the EIC. We analyzed it in slices of Q^2 and x and observed a change in event shapes from single-jet topologies at high virtualities towards more uniform shapes at small virtualities. Non-perturbative uncertainties can reach comparable size as the scale variations in limited region of the phase space and especially towards smaller virtualities. Those can to an extent be mitigated by modern grooming techniques. However, especially with the availability of NNLO FO calculations, and the advent of general NNLO matching techniques in the foreseeable future, this implies a strong necessity of understanding better non-perturbative and higher twist corrections due to the lower center-of-mass energy at the EIC than at HERA, in order to fully exploit the potential of the data. Tuning cluster and string model in comparable setups, using simultaneously LEP and DIS data, should be a pragmatic first step in this direction. Ideally, this exercise would also produce tuning uncertainties for both model tunes.

Our study showcases the state-of-the-art of precision hadron-level predictions for the EIC and examines the leading uncertainties. At virtualities of $Q^2 \approx 1\text{-}10 \text{ GeV}^2$ in NC DIS, the photoproduction region comes into play, and the merging of additional legs in the matrix elements are the tool to interpolate towards this region.

While many exclusive measurements are planned during the operation of the EIC, an understanding of the inclusive background is crucial for any analysis. Here, we showed a global analysis of the DIS region, future studies will need to understand better the photoproduction region and the interpolation between the two to fully allow inclusive jet measurements at the EIC. This would allow performing jet studies at the EIC in a fully inclusive way over all virtualities, which has so far been formulated as a goal in the experimental program, but has not seen much attention from the theoretical side. Calculations at even higher order, at NNLO and beyond, and ideally combined with either resummation or matched to the parton shower, should be within reach in the upcoming years and in time for the data-taking at the EIC.

Acknowledgments

We are grateful to Frank Krauss for encouraging us to investigate this topic and for his comments on our manuscript. D.R. is supported by the European Union under the HORIZON program in Marie Skłodowska-Curie project No. 101153541. F.S. is supported by the STFC under grant agreement ST/P006744/1. P.M. is supported by the Swiss National Science Foundation (SNF) under contract 200020-204200.

A Further Observables

In this appendix we present further observables and versions of plots that we omitted in the main text for brevity.

A.1 Neutral current 1-jettiness

Here we show the remaining 1-jettiness histograms in NC DIS in the x and Q^2 ranges from Fig. 7 with the same ratio panels as in Fig. 8.

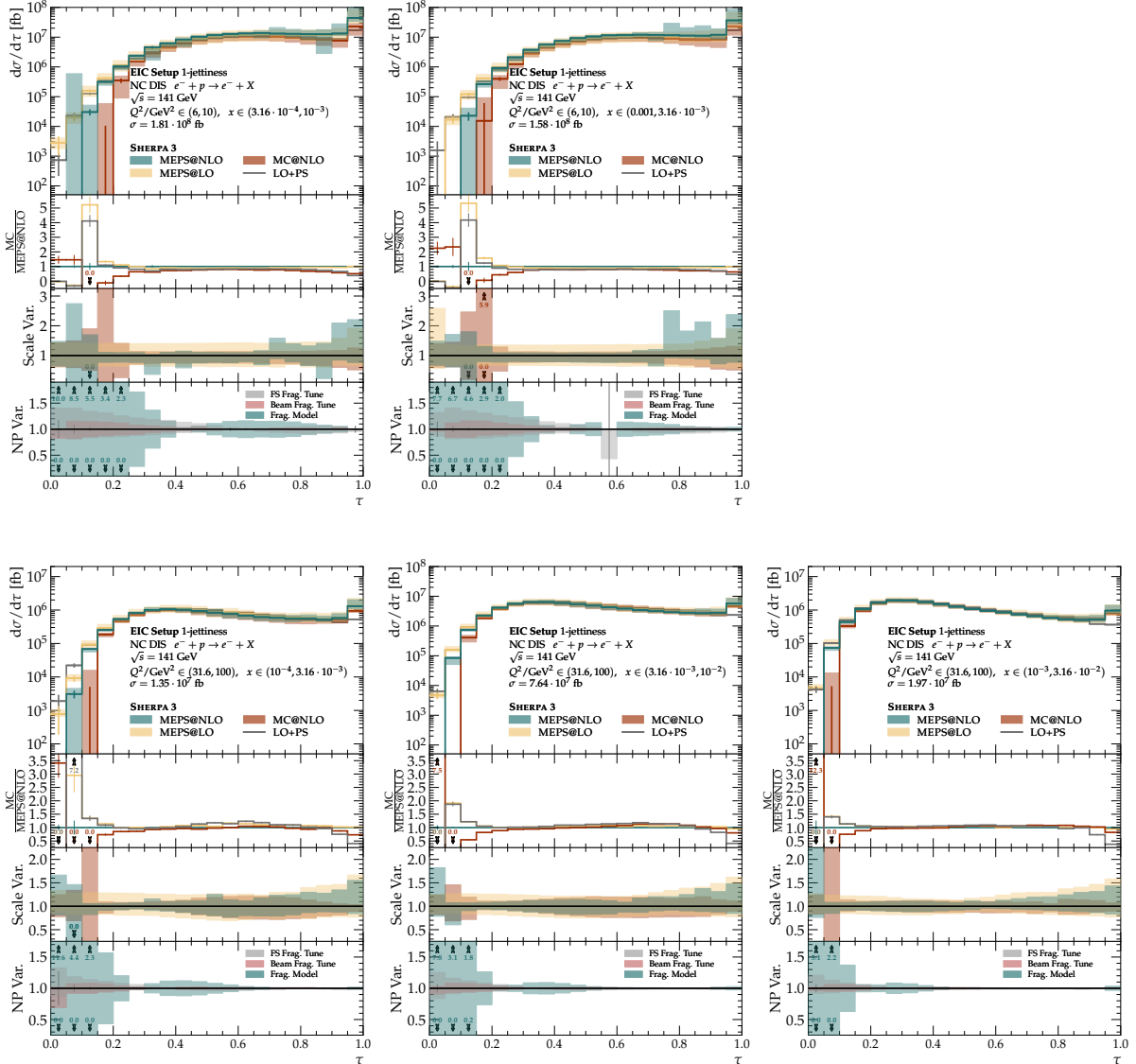


Figure 15: Differential distributions of 1-jettiness τ in a fixed slice of Q^2 and different bins of x in NC DIS at the EIC. The bottom ratios in each row indicate, from top to bottom, the ratio of each prediction to the MEPS@NLO one, the uncertainty from scale variations and the uncertainty from non-perturbative model and tuning variations. The error bars in the lowest panel indicate the statistical uncertainty of the difference between cluster and string model.

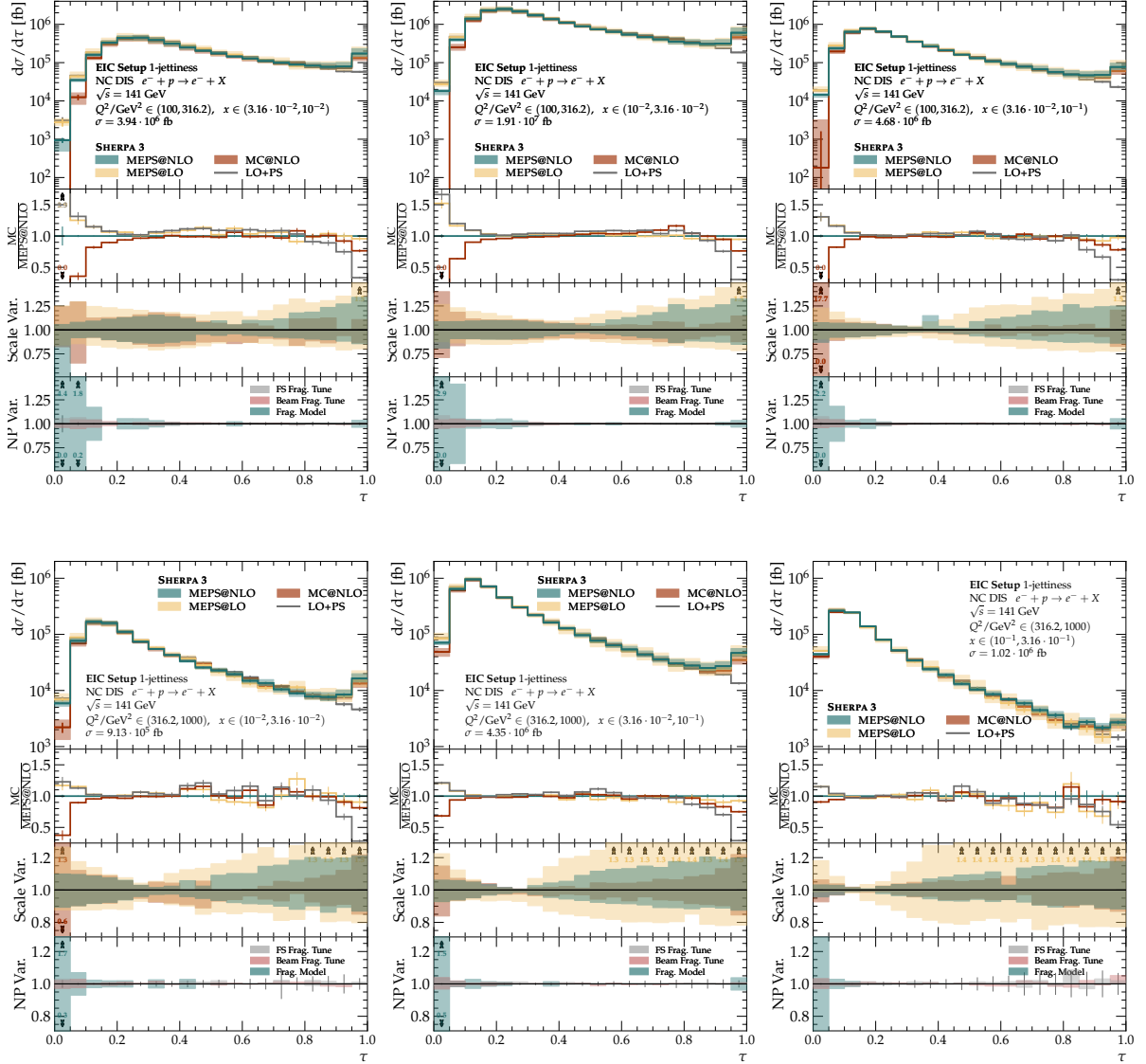


Figure 16: Differential distributions of 1-jettiness τ in a fixed slice of Q^2 and different bins of x in NC DIS at the EIC. The bottom ratios in each row indicate, from top to bottom, the ratio of each prediction to the MEPS@NLO one, the uncertainty from scale variations and the uncertainty from non-perturbative model and tuning variations. The error bars in the lowest panel indicate the statistical uncertainty of the difference between cluster and string model.

A.2 Charged current 1-jettiness

Here we show remaining the 1-jettiness observable in CC DIS in the x and Q^2 ranges from Fig. 13 with the same ratio panels as in Fig. 14.

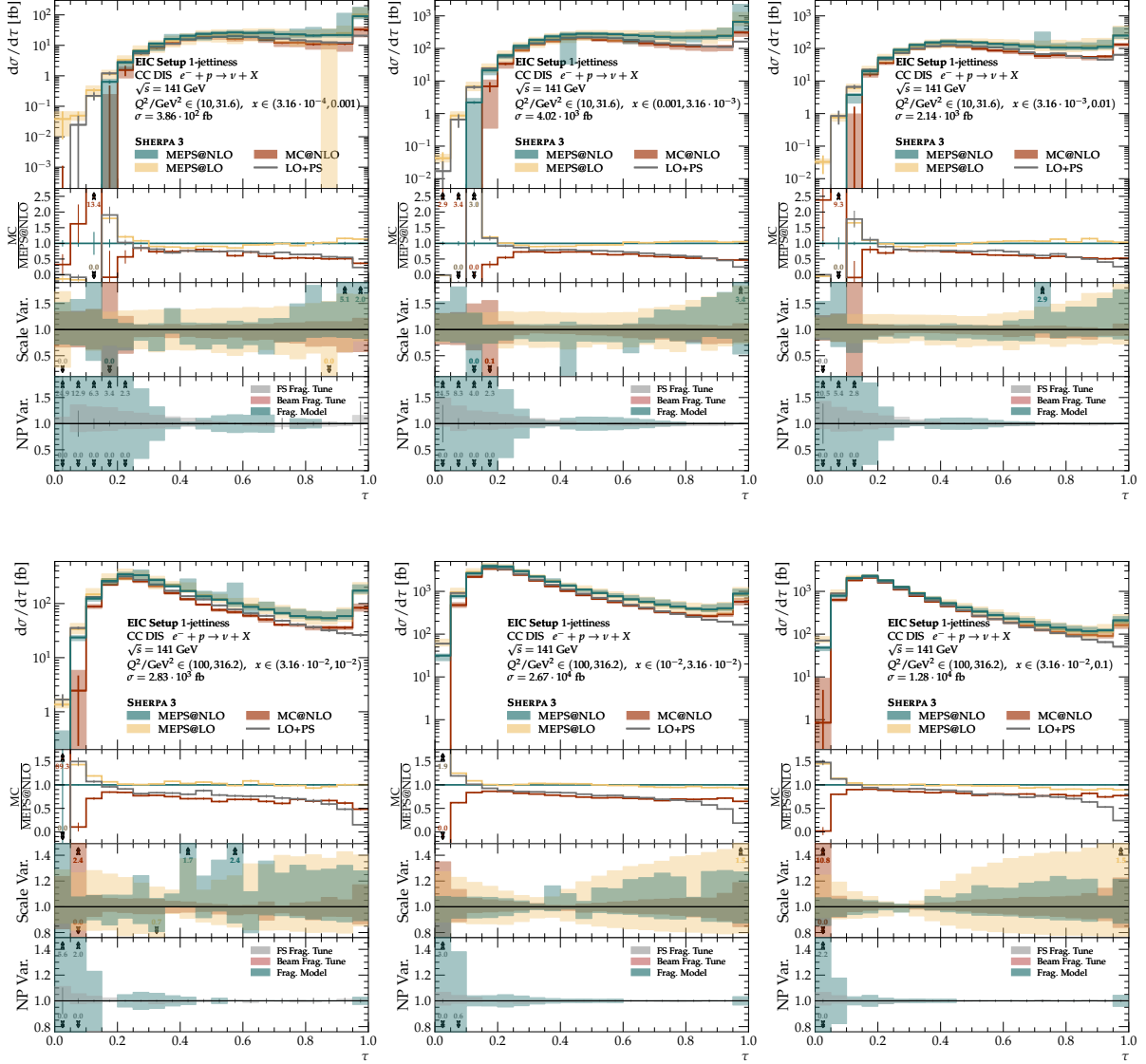


Figure 17: Differential distributions of 1-jettiness τ in a fixed slice of Q^2 and different bins of x in CC DIS at the EIC. The bottom ratios in each row indicate, from top to bottom, the ratio of each prediction to the MEPS@NLO one, the uncertainty from scale variations and the uncertainty from non-perturbative model and tuning variations. The error bars in the lowest panel indicate the statistical uncertainty of the difference between cluster and string model.

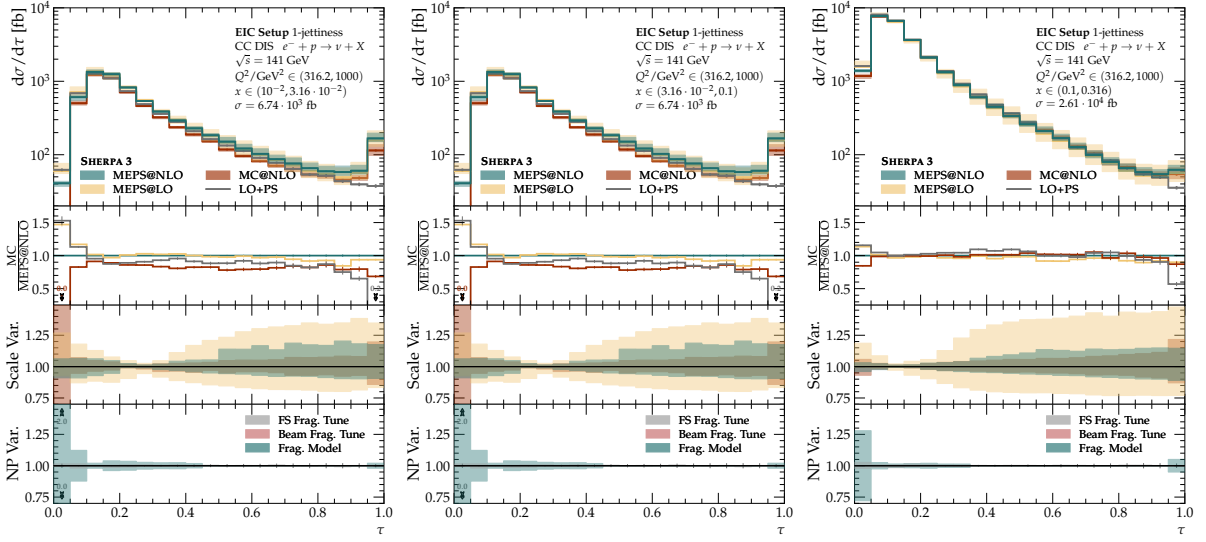


Figure 18: Differential distributions of 1-jettiness τ in a fixed slice of Q^2 and different bins of x in CC DIS at the EIC. The bottom ratios in each row indicate, from top to bottom, the ratio of each prediction to the MEPS@NLO one, the uncertainty from scale variations and the uncertainty from non-perturbative model and tuning variations. The error bars in the lowest panel indicate the statistical uncertainty of the difference between cluster and string model.

A.3 Charged current groomed 1-jettiness

In this appendix we include the equivalent of Fig. 9, presenting 1-jettiness after soft-drop grooming for CC DIS, for completeness.

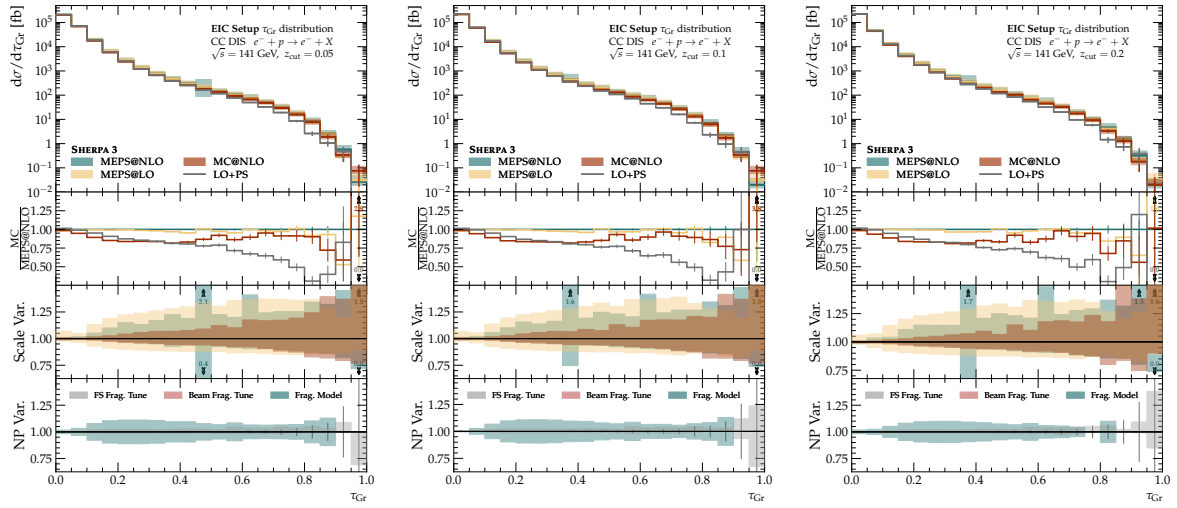


Figure 19: Groomed 1-jettiness in CC DIS at the EIC. The bottom ratios in each row indicate, from top to bottom, the ratio of each prediction to the MEPS@NLO one, the uncertainty from scale variations and the uncertainty from non-perturbative model and tuning variations. The error bars in the lowest panel indicate the statistical uncertainty of the difference between cluster and string model.

References

- [1] M. Klein and R. Yoshida, *Collider Physics at HERA*, Prog. Part. Nucl. Phys. **61** (2008), 343–393, [[arXiv:0805.3334](#) [hep-ex]].
- [2] H. Abramowicz and A. Caldwell, *HERA collider physics*, Rev. Mod. Phys. **71** (1999), 1275–1410, [[hep-ex/9903037](#)].
- [3] P. Newman and M. Wing, *The Hadronic Final State at HERA*, Rev. Mod. Phys. **86** (2014), no. 3, 1037, [[arXiv:1308.3368](#) [hep-ex]].
- [4] R. K. Ellis, H. Georgi, M. Machacek, H. D. Politzer and G. G. Ross, *Perturbation Theory and the Parton Model in QCD*, Nucl. Phys. B **152** (1979), 285–329.
- [5] J. C. Collins, D. E. Soper and G. Sterman, *Factorization of hard processes in QCD*, Adv. Ser. Direct. High Energy Phys. **5** (1988), 1–91, [[hep-ph/0409313](#)].
- [6] A. Accardi et al., *Electron Ion Collider: The Next QCD Frontier: Understanding the glue that binds us all*, Eur. Phys. J. A **52** (2016), no. 9, 268, [[arXiv:1212.1701](#) [nucl-ex]].
- [7] R. Abdul Khalek et al., *Science Requirements and Detector Concepts for the Electron-Ion Collider: EIC Yellow Report*, Nucl. Phys. A **1026** (2022), 122447, [[arXiv:2103.05419](#) [physics.ins-det]].
- [8] J. A. M. Vermaseren, A. Vogt and S. Moch, *The Third-order QCD corrections to deep-inelastic scattering by photon exchange*, Nucl. Phys. B **724** (2005), 3–182, [[hep-ph/0504242](#)].
- [9] S. Moch, J. A. M. Vermaseren and A. Vogt, *Third-order QCD corrections to the charged-current structure function $F(3)$* , Nucl. Phys. B **813** (2009), 220–258, [[arXiv:0812.4168](#) [hep-ph]].
- [10] J. Currie, T. Gehrmann, E. W. N. Glover, A. Huss, J. Niehues and A. Vogt, *N^3LO corrections to jet production in deep inelastic scattering using the Projection-to-Born method*, JHEP **05** (2018), 209, [[arXiv:1803.09973](#) [hep-ph]].
- [11] S. Höche, F. Krauss, S. Schumann and F. Siegert, *QCD matrix elements and truncated showers*, JHEP **05** (2009), 053, [[arXiv:0903.1219](#) [hep-ph]].
- [12] T. Carli, T. Gehrmann and S. Hoeche, *Hadronic final states in deep-inelastic scattering with Sherpa*, Eur. Phys. J. C **67** (2010), 73–97, [[arXiv:0912.3715](#) [hep-ph]].
- [13] S. Höche, F. Krauss, M. Schönherr and F. Siegert, *QCD matrix elements + parton showers: The NLO case*, JHEP **04** (2013), 027, [[arXiv:1207.5030](#) [hep-ph]].
- [14] T. Gehrmann, S. Höche, F. Krauss, M. Schönherr and F. Siegert, *NLO QCD matrix elements + parton showers in $e^+e^- \rightarrow \text{hadrons}$* , JHEP **01** (2013), 144, [[arXiv:1207.5031](#) [hep-ph]].
- [15] I. Helenius, J. O. Laulainen and C. T. Preuss, *Multi-jet production in deep inelastic scattering with Pythia*, JHEP **05** (2025), 153, [[arXiv:2410.20950](#) [hep-ph]].
- [16] B. S. Page, X. Chu and E. C. Aschenauer, *Experimental Aspects of Jet Physics at a Future EIC*, Phys. Rev. D **101** (2020), no. 7, 072003, [[arXiv:1911.00657](#) [hep-ph]].
- [17] Y.-T. Chien, A. Deshpande, M. M. Mondal and G. Sterman, *Probing hadronization with flavor correlations of leading particles in jets*, Phys. Rev. D **105** (2022), no. 5, L051502, [[arXiv:2109.15318](#) [hep-ph]].
- [18] M. Arratia, Y. Song, F. Ringer and B. V. Jacak, *Jets as precision probes in electron-nucleus collisions at the future Electron-Ion Collider*, Phys. Rev. C **101** (2020), no. 6, 065204, [[arXiv:1912.05931](#) [nucl-ex]].

- [19] M. Arratia, Z.-B. Kang, A. Prokudin and F. Ringer, *Jet-based measurements of Sivers and Collins asymmetries at the future electron-ion collider*, Phys. Rev. D **102** (2020), no. 7, [074015](#), [[arXiv:2007.07281](#) [hep-ph]].
- [20] L. Zheng, E. C. Aschenauer, J. H. Lee, B.-W. Xiao and Z.-B. Yin, *Accessing the gluon Sivers function at a future electron-ion collider*, Phys. Rev. D **98** (2018), no. 3, [034011](#), [[arXiv:1805.05290](#) [hep-ph]].
- [21] M. Arratia, Y. Furlotova, T. J. Hobbs, F. Olness and S. J. Sekula, *Charm jets as a probe for strangeness at the future Electron-Ion Collider*, Phys. Rev. D **103** (2021), no. 7, [074023](#), [[arXiv:2006.12520](#) [hep-ph]].
- [22] M. Arratia, Z.-B. Kang, S. J. Paul, A. Prokudin, F. Ringer and F. Zhao, *Neutrino-tagged jets at the Electron-Ion Collider*, Phys. Rev. D **107** (2023), no. 9, [094036](#), [[arXiv:2212.02432](#) [hep-ph]].
- [23] A. Banfi, S. Ferrario Ravasio, B. Jäger, A. Karlberg, F. Reichenbach and G. Zanderighi, *A POWHEG generator for deep inelastic scattering*, JHEP **02** (2024), [023](#), [[arXiv:2309.02127](#) [hep-ph]].
- [24] I. Borsa and B. Jäger, *Parton-shower effects in polarized deep inelastic scattering*, JHEP **07** (2024), [177](#), [[arXiv:2404.07702](#) [hep-ph]].
- [25] L. Buonocore, G. Limatola, P. Nason and F. Tramontano, *An event generator for Lepton-Hadron deep inelastic scattering at NLO+PS with POWHEG including mass effects*, JHEP **08** (2024), [083](#), [[arXiv:2406.05115](#) [hep-ph]].
- [26] A. Karlberg, *disorder: Deep inelastic scattering at high orders*, SciPost Phys. Codeb. **2024** (2024), [32](#), [[arXiv:2401.16964](#) [hep-ph]].
- [27] [A. Huss et al.](#), NNLOJET collaboration, *NNLOJET: a parton-level event generator for jet cross sections at NNLO QCD accuracy*, [arXiv:2503.22804](#) [hep-ph].
- [28] P. Meinzinger and F. Krauss, *Hadron-level NLO predictions for QCD observables in photo-production at the Electron-Ion Collider*, Phys. Rev. D **109** (2024), no. 3, [034037](#), [[arXiv:2311.14571](#) [hep-ph]].
- [29] [J. Andersen et al.](#), *Les Houches 2023: Physics at TeV Colliders: Standard Model Working Group Report*, [arXiv:2406.00708](#) [hep-ph].
- [30] D. Kang, C. Lee and I. W. Stewart, *Using 1-Jettiness to Measure 2 Jets in DIS 3 Ways*, Phys. Rev. D **88** (2013), [054004](#), [[arXiv:1303.6952](#) [hep-ph]].
- [31] S. Bethke et al., JADE collaboration, *Experimental Investigation of the Energy Dependence of the Strong Coupling Strength*, Phys. Lett. B **213** (1988), [235–241](#).
- [32] S. Catani, Y. L. Dokshitzer, M. H. Seymour and B. R. Webber, *Longitudinally-invariant k_{\perp} -clustering algorithms for hadron-hadron collisions*, Nucl. Phys. **B406** (1993), [187–224](#).
- [33] M. Cacciari, G. P. Salam and G. Soyez, *The Anti- $k(t)$ jet clustering algorithm*, JHEP **04** (2008), [063](#), [[arXiv:0802.1189](#) [hep-ph]].
- [34] M. Arratia, Y. Makris, D. Neill, F. Ringer and N. Sato, *Asymmetric jet clustering in deep-inelastic scattering*, Phys. Rev. D **104** (2021), no. 3, [034005](#), [[arXiv:2006.10751](#) [hep-ph]].
- [35] A. J. Larkoski, I. Moult and B. Nachman, *Jet Substructure at the Large Hadron Collider: A Review of Recent Advances in Theory and Machine Learning*, Phys. Rept. **841** (2020), [1–63](#), [[arXiv:1709.04464](#) [hep-ph]].
- [36] R. Kogler et al., *Jet Substructure at the Large Hadron Collider: Experimental Review*, Rev. Mod. Phys. **91** (2019), no. 4, [045003](#), [[arXiv:1803.06991](#) [hep-ex]].
- [37] S. Marzani, G. Soyez and M. Spannowsky, *Looking inside jets: an introduction to jet substructure and boosted-object phenomenology*, vol. 958, Springer, 2019.

- [38] S. Marzani, *Jets at Colliders*, 179–211.
- [39] A. J. Larkoski, S. Marzani, G. Soyez and J. Thaler, *Soft Drop*, JHEP **1405** (2014), [146](#), [[arXiv:1402.2657](#)] [hep-ph].
- [40] J. Baron, D. Reichelt, S. Schumann, N. Schwanemann and V. Theeuwes, *Soft-drop grooming for hadronic event shapes*, JHEP **07** (2021), [142](#), [[arXiv:2012.09574](#)] [hep-ph].
- [41] J. Baron, S. Marzani and V. Theeuwes, *Soft-Drop Thrust*, JHEP **08** (2018), [105](#), [[arXiv:1803.04719](#)] [hep-ph], [Erratum: JHEP 05, 056 (2019)].
- [42] S. Marzani, D. Reichelt, S. Schumann, G. Soyez and V. Theeuwes, *Fitting the Strong Coupling Constant with Soft-Drop Thrust*, JHEP **11** (2019), [179](#), [[arXiv:1906.10504](#)] [hep-ph].
- [43] A. Gehrmann-De Ridder, C. T. Preuss, D. Reichelt and S. Schumann, *NLO+NLL' accurate predictions for three-jet event shapes in hadronic Higgs decays*, JHEP **07** (2024), [160](#), [[arXiv:2403.06929](#)] [hep-ph].
- [44] Y.-T. Chien, O. Fedkevych, D. Reichelt and S. Schumann, *Jet angularities in dijet production in proton-proton and heavy-ion collisions at RHIC*, JHEP **07** (2024), [230](#), [[arXiv:2404.04168](#)] [hep-ph].
- [45] Y. Makris, *Revisiting the role of grooming in DIS*, Phys. Rev. D **103** (2021), no. 5, [054005](#), [[arXiv:2101.02708](#)] [hep-ph].
- [46] V. Andreev et al., H1 collaboration, *Measurement of groomed event shape observables in deep-inelastic electron-proton scattering at HERA*, Eur. Phys. J. C **84** (2024), no. 7, [718](#), [[arXiv:2403.10134](#)] [hep-ex].
- [47] E. Bothmann et al., Sherpa collaboration, *Event generation with Sherpa 3*, JHEP **12** (2024), [156](#), [[arXiv:2410.22148](#)] [hep-ph].
- [48] F. Krauss, R. Kuhn and G. Soff, *AMEGIC++ 1.0: A Matrix Element Generator In C++*, JHEP **02** (2002), [044](#), [[hep-ph/0109036](#)].
- [49] T. Gleisberg and S. Höche, *Comix, a new matrix element generator*, JHEP **12** (2008), [039](#), [[arXiv:0808.3674](#)] [hep-ph].
- [50] S. Schumann and F. Krauss, *A parton shower algorithm based on Catani-Seymour dipole factorisation*, JHEP **03** (2008), [038](#), [[arXiv:0709.1027](#)] [hep-ph].
- [51] S. Catani and M. H. Seymour, *A general algorithm for calculating jet cross sections in NLO QCD*, Nucl. Phys. **B485** (1997), [291–419](#), [[hep-ph/9605323](#)].
- [52] S. Frixione and B. R. Webber, *Matching NLO QCD computations and parton shower simulations*, JHEP **06** (2002), [029](#), [[hep-ph/0204244](#)].
- [53] S. Catani, F. Krauss, R. Kuhn and B. R. Webber, *QCD matrix elements + parton showers*, JHEP **11** (2001), [063](#), [[hep-ph/0109231](#)].
- [54] B. R. Webber, *A QCD model for jet fragmentation including soft gluon interference*, Nucl. Phys. **B238** (1984), [492](#).
- [55] J.-C. Winter, F. Krauss and G. Soff, *A modified cluster-hadronisation model*, Eur. Phys. J. **C36** (2004), [381–395](#), [[hep-ph/0311085](#)].
- [56] G. S. Chahal and F. Krauss, *Cluster Hadronisation in Sherpa*, SciPost Phys. **13** (2022), no. 2, [019](#), [[arXiv:2203.11385](#)] [hep-ph].
- [57] C. Bierlich et al., *A comprehensive guide to the physics and usage of PYTHIA 8.3*, SciPost Phys. Codeb. **2022** (2022), [8](#), [[arXiv:2203.11601](#)] [hep-ph].

- [58] C. Bierlich et al., *Robust Independent Validation of Experiment and Theory: Rivet version 3*, SciPost Phys. **8** (2020), 026, [[arXiv:1912.05451](#)] [hep-ph].
- [59] S. Höche, F. Krauss, M. Schönherr and F. Siegert, *A critical appraisal of NLO+PS matching methods*, JHEP **09** (2012), 049, [[arXiv:1111.1220](#)] [hep-ph].
- [60] S. Catani, S. Dittmaier, M. H. Seymour and Z. Trocsanyi, *The dipole formalism for next-to-leading order QCD calculations with massive partons*, Nucl. Phys. **B627** (2002), 189–265, [[hep-ph/0201036](#)].
- [61] R. D. Ball et al., NNPDF collaboration, *Parton distributions for the LHC Run II*, JHEP **04** (2015), 040, [[arXiv:1410.8849](#)] [hep-ph].
- [62] A. Buckley, J. Ferrando, S. Lloyd, K. Nordström, B. Page, M. Rüfenacht, M. Schönherr and G. Watt, *LHAPDF6: parton density access in the LHC precision era*, Eur. Phys. J. **C75** (2015), 132, [[arXiv:1412.7420](#)] [hep-ph].
- [63] M. Cacciari and N. Houdeau, *Meaningful characterisation of perturbative theoretical uncertainties*, JHEP **09** (2011), 039, [[arXiv:1105.5152](#)] [hep-ph].
- [64] C. Duhr, A. Huss, A. Mazeliauskas and R. Szafron, *An analysis of Bayesian estimates for missing higher orders in perturbative calculations*, JHEP **09** (2021), 122, [[arXiv:2106.04585](#)] [hep-ph].
- [65] A. Ghosh, B. Nachman, T. Plehn, L. Shire, T. M. P. Tait and D. Whiteson, *Statistical patterns of theory uncertainties*, SciPost Phys. Core **6** (2023), 045, [[arXiv:2210.15167](#)] [hep-ph].
- [66] **F. J. Tackmann**, *Beyond Scale Variations: Perturbative Theory Uncertainties from Nuisance Parameters*, [arXiv:2411.18606](#) [hep-ph].
- [67] **M. A. Lim and R. Poncelet**, *Robust estimates of theoretical uncertainties at fixed-order in perturbation theory*, [arXiv:2412.14910](#) [hep-ph].
- [68] S. Höche, D. Reichelt and F. Siegert, *Momentum conservation and unitarity in parton showers and NLL resummation*, JHEP **01** (2018), 118, [[arXiv:1711.03497](#)] [hep-ph].
- [69] E. Bothmann, M. Schönherr and S. Schumann, *Reweighting QCD matrix-element and parton-shower calculations*, Eur. Phys. J. **C76** (2016), no. 11, 590, [[arXiv:1606.08753](#)] [hep-ph].
- [70] M. Knobbe, F. Krauss, D. Reichelt and S. Schumann, *Measuring hadronic Higgs boson branching ratios at future lepton colliders*, Eur. Phys. J. **C84** (2024), no. 1, 83, [[arXiv:2306.03682](#)] [hep-ph].
- [71] M. Knobbe, D. Reichelt and S. Schumann, *(N)NLO+NLL' accurate predictions for plain and groomed 1-jettiness in neutral current DIS*, JHEP **09** (2023), 194, [[arXiv:2306.17736](#)] [hep-ph].
- [72] D. Reichelt, S. Caletti, O. Fedkevych, S. Marzani, S. Schumann and G. Soyez, *Phenomenology of jet angularities at the LHC*, JHEP **03** (2022), 131, [[arXiv:2112.09545](#)] [hep-ph].
- [73] S. Chekanov et al., ZEUS collaboration, *Multi-jet cross-sections in charged current $e^\pm p$ scattering at HERA*, Phys. Rev. D **78** (2008), 032004, [[arXiv:0802.3955](#)] [hep-ex].
- [74] V. Andreev et al., H1 collaboration, *Unbinned deep learning jet substructure measurement in high Q^2 $e-p$ collisions at HERA*, Phys. Lett. B **844** (2023), 138101, [[arXiv:2303.13620](#)] [hep-ex].
- [75] V. Andreev et al., H1 collaboration, *Observation and differential cross section measurement of neutral current DIS events with an empty hemisphere in the Breit frame*, Eur. Phys. J. **C84** (2024), no. 7, 720, [[arXiv:2403.08982](#)] [hep-ex].
- [76] V. Andreev et al., H1 collaboration, *Measurement of the 1-jettiness event shape observable in deep-inelastic electron-proton scattering at HERA*, Eur. Phys. J. **C84** (2024), no. 8, 785, [[arXiv:2403.10109](#)] [hep-ex].

- [77] [V. Andreev et al.](#), H1 collaboration, *Machine Learning-Assisted Measurement of Lepton-Jet Azimuthal Angular Asymmetries in Deep-Inelastic Scattering at HERA*, [arXiv:2412.14092](#) [hep-ex].
- [78] M. Knobbe, D. Reichelt, S. Schumann and L. Stöcker, *Precision calculations for groomed event shapes at HERA*, PoS **DIS2024** (2025), **172**, [[arXiv:2407.02456](#)] [hep-ph].
- [79] U. Amaldi (Ed.), *Study of an ep Facility for Europe DESY, Hamburg, April 2-3, 1979.*, vol. 790402, Hamburg, Germany, Deutsches Electron Synchrotron / European Committee for Future Accelerators, 1979.
- [80] H1 collaboration, *Towards Unfolding All Particles in High Q^2 DIS Events*, H1prelim-25-031, DIS 2025.
- [81] M. Dasgupta and G. P. Salam, *Resummed event shape variables in DIS*, JHEP **08** (2002), **032**, [[hep-ph/0208073](#)] [hep-ph].
- [82] [J.-H. Ee](#), [D. Kang](#), [C. Lee](#) and [I. W. Stewart](#), *Precision DIS thrust predictions for HERA and EIC*, [arXiv:2504.05234](#) [hep-ph].